THE JOURNAL OF BIOLOGICAL CHEMISTRY VOL. 291, NO. 45, pp. 23719–23733, November 4, 2016

Identification and Characterization of MCM3 as a Kelch-like ECH-associated Protein 1 (KEAP1) Substrate*[S]

Received for publication, April 8, 2016, and in revised form, September 12, 2016 Published, JBC Papers in Press, September 12, 2016, DOI 10.1074/jbc.M116.729418

Kathleen M. Mulvaney[‡§], Jacob P. Matson[¶], Priscila F. Siesser[§], Tigist Y. Tamir[§‖], Dennis Goldfarb[§], Timothy M. Jacobs[‡‡], Erica W. Cloer[‡§], Joseph S. Harrison[§¶], Cyrus Vaziri[§ §§], Jeanette G. Cook[§¶1], and Michael B. Major[‡§‖**2]**

*From the Departments of [‡]Cell Biology and Physiology, [¶]Biochemistry and Biophysics, [‖]Pharmacology, **Computer Science, and [§§]Pathology, [§]Lineberger Comprehensive Cancer Center, and [‡‡]Eshelman School of Pharmacy, University of North Carolina, Chapel Hill, North Carolina 27599*

KEAP1 is a substrate adaptor protein for a CUL3-based E3 ubiquitin ligase. Ubiquitylation and degradation of the antioxidant transcription factor NRF2 is considered the primary function of KEAP1; however, few other KEAP1 substrates have been identified. Because KEAP1 is altered in a number of human pathologies and has been proposed as a potential therapeutic target therein, we sought to better understand KEAP1 through systematic identification of its substrates. Toward this goal, we combined parallel affinity capture proteomics and candidate-based approaches. Substrate-trapping proteomics yielded NRF2 and the related transcription factor NRF1 as KEAP1 substrates. Our targeted investigation of KEAP1-interacting proteins revealed MCM3, an essential subunit of the replicative DNA helicase, as a new substrate. We show that MCM3 is ubiquitylated by the KEAP1-CUL3-RBX1 complex in cells and *in vitro*. Using ubiquitin remnant profiling, we identify the sites of KEAP1-dependent ubiquitylation in MCM3, and these sites are on predicted exposed surfaces of the MCM2–7 complex. Unexpectedly, we determined that KEAP1 does not regulate total MCM3 protein stability or subcellular localization. Our analysis of a KEAP1 targeting motif in MCM3 suggests that MCM3 is a point of direct contact between KEAP1 and the MCM hexamer. Moreover, KEAP1 associates with chromatin in a cell cycle-dependent fashion with kinetics similar to the MCM2–7 complex. KEAP1 is thus poised to affect MCM2–7 dynamics or function rather than MCM3 abundance. Together, these data establish new functions for KEAP1 within the nucleus and identify MCM3 as a novel substrate of the KEAP1-CUL3-RBX1 E3 ligase.

Kelch-like ECH-associated protein 1 (KEAP1)[3] is a substrate adaptor protein for a Cullin3 (CUL3)-RBX1 E3 ubiquitin ligase complex (1–3). Recent studies have described the molecular architecture and mechanism for the KEAP1-CUL3-RBX1 ubiquitylation machine (4, 5). The most well studied and established substrate of the KEAP1 complex is the NFE2L2 transcription factor (henceforth referred to as NRF2) (1–3, 6, 7). A homodimer of KEAP1 tethered to CUL3 via its amino-terminal bric-a-brac/tramtrack/broad complex (BTB) domains binds to a single molecule of NRF2, and the C-terminal kelch domains of a KEAP1 homodimer bind to a high-affinity motif (ETGE) and a lower-affinity motif (DLG) within the NRF2 protein (2, 8, 9). Under homeostatic conditions, ubiquitylated NRF2 is rapidly degraded by the proteasome, having a half-life of less than 30 min (10). KEAP1 acts as a sensor of cellular reduction-oxidation (redox) state through its 27 cysteine residues (6, 11, 12). The reactive cysteine residues within KEAP1 can be modified by reactive oxygen species (ROS), which is thought to trigger a conformational change in the KEAP1 complex (3, 6, 11). As a result, NRF2 is no longer efficiently degraded and thus accumulates, translocates to the nucleus, and promotes the transcription of antioxidant and cytoprotective genes (10, 13, 14). Specifically, nuclear NRF2 forms heterodimers with small Maf proteins, and together they bind to the antioxidant response elements within the promoter region of NRF2 target genes, which include free radical scavengers, glutathione synthesis genes, and xenobiotic efflux proteins (7, 10, 15, 16). The up-regulation of NRF2 target genes mitigates oxidative stress and confers resistance to a number of toxins, including chemotherapeutics (7, 13, 17, 18). The KEAP1-NRF2 signaling pathway serves as the primary defense of the cell against oxidative stress (13, 14).

Although NRF2 degradation has long been thought to be the primary function of KEAP1, we have shown that KEAP1 associates with a number of interesting and diverse proteins, suggesting previously unknown roles for KEAP1 (19, 20). In support of this concept, three substrates have recently been

* This work was supported by a grant from the Sidney Kimmel Cancer Foundation (to M. B. M.), by American Cancer Society Grant RSG-14-068-01-TBE (to M. B. M.), by National Science Foundation Graduate Research Fellowship DGE-1144081 (to J. P. M.), and by NIGMS, National Institutes of Health Grant R01GM102413 (to J. G. C.). The authors declare that they have no conflicts of interest with the contents of this article. The content is solely the responsibility of the authors and does not necessarily represent the official views of the National Institutes of Health.

[S] This article contains supplemental Tables S1–S3.

The mass spectrometry proteomics data have been deposited in the ProteomeXchange Consortium via the PRIDE partner repository with the dataset identifier PXD003929.

[1] To whom correspondence may be addressed: Dept. of Biochemistry and Biophysics, 120 Mason Farm Rd., Campus Box 7260, Chapel Hill, NC 27599-7260. Tel.: 919-843-3867; E-mail: jgcook@email.unc.edu.

[2] To whom correspondence may be addressed: Dept. of Cell Biology and Physiology, Lineberger Comprehensive Cancer Center, University of North Carolina, 450 West Dr., Lineberger Bldg., CB#7295, Chapel Hill, NC 27599-7295. Tel.: 919-259-2695; E-mail: benmajor@med.unc.edu.

[3] The abbreviations used are: KEAP, kelch-like ECH-associated protein; redox, reduction-oxidation; ROS, reactive oxygen species; PAC, parallel affinity capture; SBP, streptavidin binding peptide; IP, immunoprecipitation; PLA, proximity ligation assay; tBHQ, *tert*-butylhydroquinone; AP, affinity purification; MEF, mouse embryonic fibroblast; RIPA, radioimmune precipitation assay; VSV, vesicular stomatitis virus; FDR, false discovery rate; TRITC, tetramethylrhodamine isothiocyanate.

reported for the KEAP1 E3 ligase: IKBKB (21), PGAM5 (22), and PALB2 (23). All three substrates contain an ETGE or ESGE motif that is essential for their interactions with and ubiquitylation by KEAP1. Although we have a strong understanding of the dynamics and regulation of NRF2 as a KEAP1 substrate, these other substrates are less well studied. IKBKB is reported to be a KEAP1 substrate targeted for autophagy-mediated degradation, PGAM5 is thought to be ubiquitylated and targeted to the proteasome, and KEAP1-mediated PALB2 ubiquitylation regulates its function by blocking its interaction with BRCA1 (21–24). Thus, the KEAP1-CUL3-RBX1 ligase is capable of ubiquitylating its substrates to regulate substrate stability through either proteasome-mediated or autophagy-mediated degradation or to regulate substrate function by directing protein-protein interactions.

In addition to the vital role the pathway plays in normal physiology, perturbations in KEAP1-NRF2 signaling have been reported in a variety of diseases, including cancer and inflammatory, cardiovascular, and neurodegenerative diseases (25–34). Most notably, sequencing efforts have determined that ~30% of non-small cell lung cancer tumors harbor mutations in the KEAP1-NRF2 pathway, and 12–15% of non-small cell lung cancer patient tumors have mutations within KEAP1 (20, 35–38). The high mutation frequency suggests a role for KEAP1-NRF2 in cancer progression. KEAP1 loss is thought to promote tumorigenesis through hyperactivation of NRF2, although little is known about other effects of KEAP1 mutation or loss. A better understanding of KEAP1 substrates would enhance our understanding of both normal KEAP1 function and of KEAP1-mutant tumors. We sought to define new KEAP1 substrates and to determine the function of their ubiquitylation by KEAP1.

Here we identify a subunit of the replicative DNA helicase minichromosome maintenance 3 (MCM3) as a KEAP1 substrate. We selected it from our set of potential KEAP1 substrates for further study based on its important role in cell cycle regulation. Interestingly, human MCM subunits do not undergo ubiquitin-mediated proteolysis during normal proliferation; instead, the chromatin loading of the MCM complex is tightly controlled during the cell cycle to ensure once-per-cell cycle genome duplication. MCM complexes are chromatin-loaded strictly during G_1 phase, activated in S phase, and progressively unloaded as DNA replication forks terminate (reviewed in Ref. 39–41). The MCM2–7 complex is extensively modified by posttranslational modifications (42–48), and, in particular, recent studies linked polyubiquitylation of the MCM7 subunit to MCM unloading in both *Saccharomyces cerevisiae* and *Xenopus laevis* (49–52). In *S. cerevisiae*, the SCF^{Dia2} ligase ubiquitylates MCM7, and in *X. laevis*, MCM7 is ubiquitylated by an unidentified cullin family member (49, 50). Thus, interaction with and polyubiquitylation by KEAP1 represents a potentially novel form of MCM regulation. We suggest that our discovery of KEAP1-mediated MCM3 ubiquitylation establishes a physical link between a key player in the oxidative stress response and chromosome replication.

Results

Identification of MCM3 as a KEAP1 Substrate—We used two complementary strategies to identify proteins ubiquitylated by the KEAP1-CUL3-RBX1 complex. First, we employed parallel affinity capture (PAC) mass spectrometry (Fig. 1*A*) (53). E3 ubiquitin ligases are processive in action: binding, ubiquitylating and releasing substrates. As such, traditional purification of E3 ligases often fails to identify the transient interactions of co-complexed substrates. The PAC approach uses genetic or pharmacological tools to block substrate degradation, which results in stabilization of the E3-substrate interaction (53). HEK293T cells engineered for stable expression of KEAP1 fused with streptavidin binding peptide (SBP) and HA epitope were grown in stable isotope labeling with amino acids in cell culture (SILAC)-light medium or SILAC-heavy medium before addition of vehicle or MG132 proteasome inhibitor (Fig. 1*A*). Mass spectrometry analysis of streptavidin-purified protein complexes from these cells revealed SILAC ratios for KEAP1 and KEAP1-associated proteins (Fig. 1*B* and supplemental Table S1). As expected, NRF2 abundance increased within the KEAP1 complex following MG132 treatment (SILAC ratio, ~4). The NRF2-related transcription factor NFE2L1 (henceforth referred to as NRF1) similarly increased within the KEAP1 complex following proteasome inhibition, suggesting that it is also a KEAP1 substrate (SILAC ratio, ~2). NRF1 is an established KEAP1-associated protein but, surprisingly, has not been reported previously to be a KEAP1 substrate (54, 55). With the exception of NRF2 and NRF1, PAC-based analysis of the KEAP1 protein complex did not reveal new putative substrates. PGAM5 is ubiquitylated by KEAP1 and targeted for proteasome-dependent degradation (22). Unexpectedly, PGAM5 did not accumulate in cell lysates or on KEAP1 following proteasome inhibition. Additionally, other high-confidence KEAP1-interacting proteins that contain an E(T/S)GE motif also did not show increased binding to KEAP1 with proteasome inhibition.

We hypothesized that, although successful for identifying rapidly catalyzed substrates, the PAC-based method may fail to reveal KEAP1 substrates with slower rates of ubiquitylation. Additionally, by design, the PAC method does not identify E3 substrates that are not bound for the proteasome. Therefore, in a second approach, we interrogated KEAP1-interacting proteins that contain an ETGE or ESGE motif. Specifically, SBPHA-KEAP1 was affinity-purified from HEK293T cells over a time course of MG132 treatment. Co-complexed proteins were quantified by LI-COR-based immunoblotting. Two patterns were observed. The class 1 proteins NRF1 and NRF2 increased rapidly in whole cell lysates and within the purified KEAP1 protein complex (~5-fold and ~18-fold, respectively) (Fig. 1, *C* and *D*). Class 2 proteins include the known KEAP1 substrate PGAM5 as well as MCM3, SLK, and MAD2L1. Although the steady-state abundances of these proteins were not affected by MG132 treatment, they reproducibly demonstrated a modest increase in KEAP1 binding (<2-fold) between 4 and 6 h of MG132 treatment. DPP3, another ETGE-containing KEAP1 interactor, did not fall into either class. Rather, it

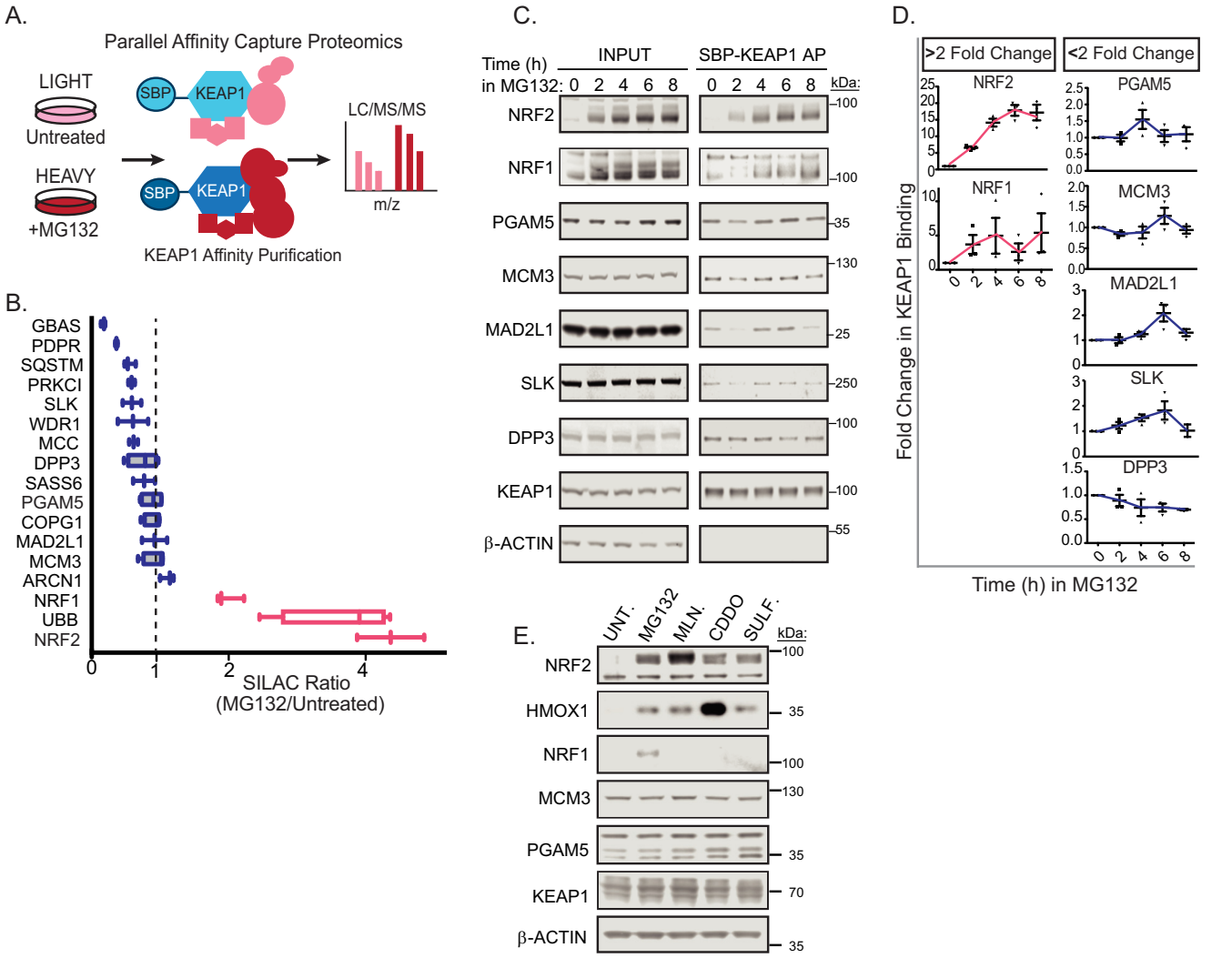

FIGURE 1. **PAC proteomics and a candidate-based approach reveal putative KEAP1 substrates.** *A*, experimental schematic for the KEAP1 PAC proteomics. Putative substrates increase in association with KEAP1 following proteasome inhibition (*red circles*). *B*, the mean SILAC ratios (heavy/light) of high-confidence KEAP1 interactors detected by streptavidin AP of SBPHA-KEAP1 followed by LC/MS-MS in the presence or absence of 2–4 h of proteasome inhibitor (MG132) are plotted (high-confidence interactors were determined by the Spotlite-scored KEAP1 interaction network (74)). Proteins plotted were detected in at least two experimental replicates. *Pink* box-and-whisker plots show proteins with increased association with KEAP1 under proteasome inhibition (increased >50%) (supplemental Table S1). *C*, Western blot analysis of streptavidin affinity-purified KEAP1 protein complexes across an MG132 time course (0–8 h). *D*, LI-COR-based quantification of data shown in *C*. The abundance of each KEAP1-interacting protein within the KEAP1 AP protein complex across three biological replicate experiments is shown. *Error bars* represent standard error of the mean. *E*, Western blotting analysis of HDF-Tert cell lysates treated with the indicated proteasome inhibitor or KEAP1-CUL3 antagonist for 6 h. Each experiment (*B–E*) was performed three to five times. *UNT*, untreated.

decreased modestly within the KEAP1 complex during proteasome inhibition.

Although both NRF1 and NRF2 responded rapidly to proteasome inhibition, NRF2 is the only KEAP1 substrate that robustly accumulated in response to treatment with a ROS mimetic (sulforaphane) or KEAP1-CUL3 antagonist (MLN4924, bardoxolone methyl (CDDO-me)) (Fig. 1*E*). Collectively, these results suggest two distinct classes of putative KEAP1 substrates: NRF1 and NRF2, which are short-lived, stress-responsive proteins that are rapidly turned over by the proteasome, and a second, more stable and higher abundance class of KEAP1 substrates comprised of PGAM5, MCM3, SLK, and MAD2L1. We chose MCM3, a member of the essential DNA replicative helicase, for further study based on its important role in cell cycle regulation.

Biochemical Analysis of the KEAP1-MCM3 Complex—Having previously identified MCM3 as a high-confidence KEAP1-interacting protein by affinity purification (AP)/MS (19, 20) and now as a putative substrate (Fig. 1, *C* and *D*), we sought to validate and determine the localization of this interaction. We first conducted a reciprocal MCM3 IP/MS experiment with ectopically expressed FLAG epitope-tagged MCM3 and detected endogenous KEAP1 in addition to all expected MCM3-associated proteins, largely those important for DNA replication (Fig. 2*A*). We also detected KEAP1 interaction with the MCM complex by endogenous co-immunoprecipitation using antibodies to MCM3 or MCM2 (another subunit of the MCM2–7 heterohexameric complex) (Fig. 2, *B* and *C*). Next, we expressed a KEAP1 fusion to a biotin ligase proximity detector, BirA*, and tested MCM subunits for *in vivo* biotinylation. We detected biotin-stimulated modification of both endogenous MCM3 and MCM2 only in cells expressing the KEAP1-BirA* fusion, demonstrating its close proximity to the MCM hexamer (Fig. 2*D*). We next assessed where in the cell KEAP1

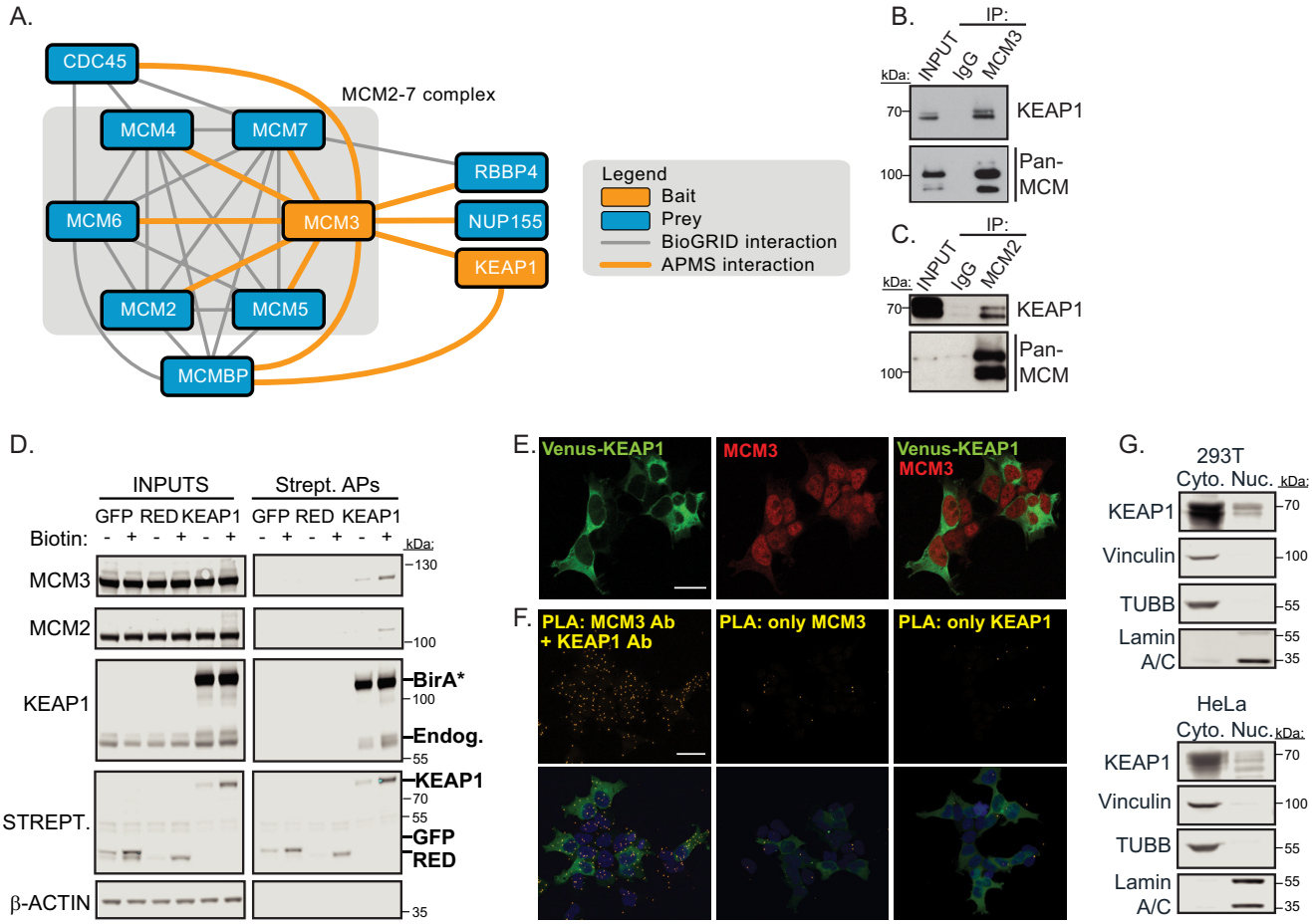

FIGURE 2. **KEAP1 associates with MCM3 in the MCM2–7 complex in both the nucleus and cytoplasm.** *A*, FLAG-KEAP1 and FLAG-MCM3 protein interaction networks were determined by FLAG IP/MS. Spotlite-scored high-confidence interactors are shown (supplemental Table S2). *B*, endogenous MCM3 IP was probed for KEAP1 and MCM proteins using an antibody to an epitope common to multiple MCM subunits. *C*, endogenous MCM2 IP was probed for KEAP1 and MCM proteins. *D*, HEK293T cells stably expressing BirA*-KEAP1 (a biotin ligase proximity detector) or cells stably expressing controls (BirA*-GFP or BirA*-HC Red (*RED*)) were subjected to streptavidin affinity purification and probed for the indicated proteins. Biotinylated proteins were detected using fluorescently labeled streptavidin (*Strept*). *Endog*, endogenous. *E*, HEK293T immunofluorescence of VENUS-KEAP1 and endogenous MCM3. *Scale bar* = 20 μm. *F*, Duo-Link *in situ* proximity ligation assay of KEAP1 and MCM3. Images represent maximum intensity projections of Z-stacks. Each *yellow* fluorescent dot represents a single interaction between KEAP1 and MCM3 (*left panel*). VENUS-KEAP1 is shown in *green*. DAPI stain for nuclei is shown in *blue*. The *center* and *right panels* are the negative controls. For clarity, the *yellow* PLA puncta are shown alone in the *top panels*. Images were acquired using a confocal microscope. *Scale bar* = 20 μm. *G*, Western blotting analysis of cytoplasmic (*Cyto*) and nuclear (*Nuc*) fractions of HEK293T and HeLa cells to determine the localization of KEAP1. β-Tubulin, Vinculin, and Lamin A/C served as controls for cell fractionation. Each experiment (*A–G*) is representative of two to three biological replicates.

and MCM3 interact. Immunofluorescence analysis using antibodies against MCM3 in cells stably expressing VENUS-KEAP1 revealed that MCM3 was mainly nuclear, but a small fraction of MCM3 antibody reactivity diffusely localized to the cytosol, in contrast to VENUS-KEAP1, which was mainly cytoplasmic with a small pool in the nucleus (Fig. 2*E*). To test in which compartment(s) KEAP1 and MCM3 associate, we performed an *in situ* proximity ligation assay (PLA) using primary antibodies for KEAP1 and MCM3. Fig. 2*F* shows representative images for this assay, demonstrating that KEAP1 and MCM3 are in close proximity to one another in both the nucleus and cytoplasm. Using subcellular fractionation followed by Western blotting, we observed that a small fraction of KEAP1 was indeed in the nucleus, in agreement with our microscopy analysis and other reports that ~5% of KEAP1 is nuclear (Fig. 2*G*) (56).

MCM3 Is a KEAP1 Substrate for Ubiquitylation in Vivo and in Vitro—Next we tested whether KEAP1 directly ubiquitylates MCM3. Under near-denaturing conditions, FLAG-MCM3 or FLAG-NRF2 was immunoprecipitated from HEK293T cells expressing control GFP or KEAP1. Western blotting analysis showed strong induction of MCM3 ubiquitylation by KEAP1, similar to the positive control NRF2 (Fig. 3, *A* and *B*). Reciprocally, siRNA-mediated silencing of KEAP1 suppressed ubiquitylation of FLAG-MCM3 (Fig. 3*C*). The degree of KEAP1 silencing by the three independent siRNAs strongly correlated with loss of MCM3 ubiquitylation. To evaluate the ubiquitylation of endogenous MCM3, we immunoprecipitated MCM3 under near-denaturing conditions from cells transfected with siRNAs targeting KEAP1 or CUL3. Both KEAP1 and CUL3 silencing suppressed ubiquitylation of endogenous MCM3 (Fig. 3*D*). These data demonstrate that the KEAP1-CUL3-RBX1 ligase is responsible for the majority of MCM3 ubiquitylation in proliferating cells. As expected, ubiquitylation of MCM3 by KEAP1 required MCM3-KEAP1 physical interaction. Specifically, we mutated the ETGE motif within MCM3 to EAAE and found that this mutant was not ubiquitylated by KEAP1 and did not bind KEAP1 (Fig. 3, *E* and *F*). Together, these data suggest

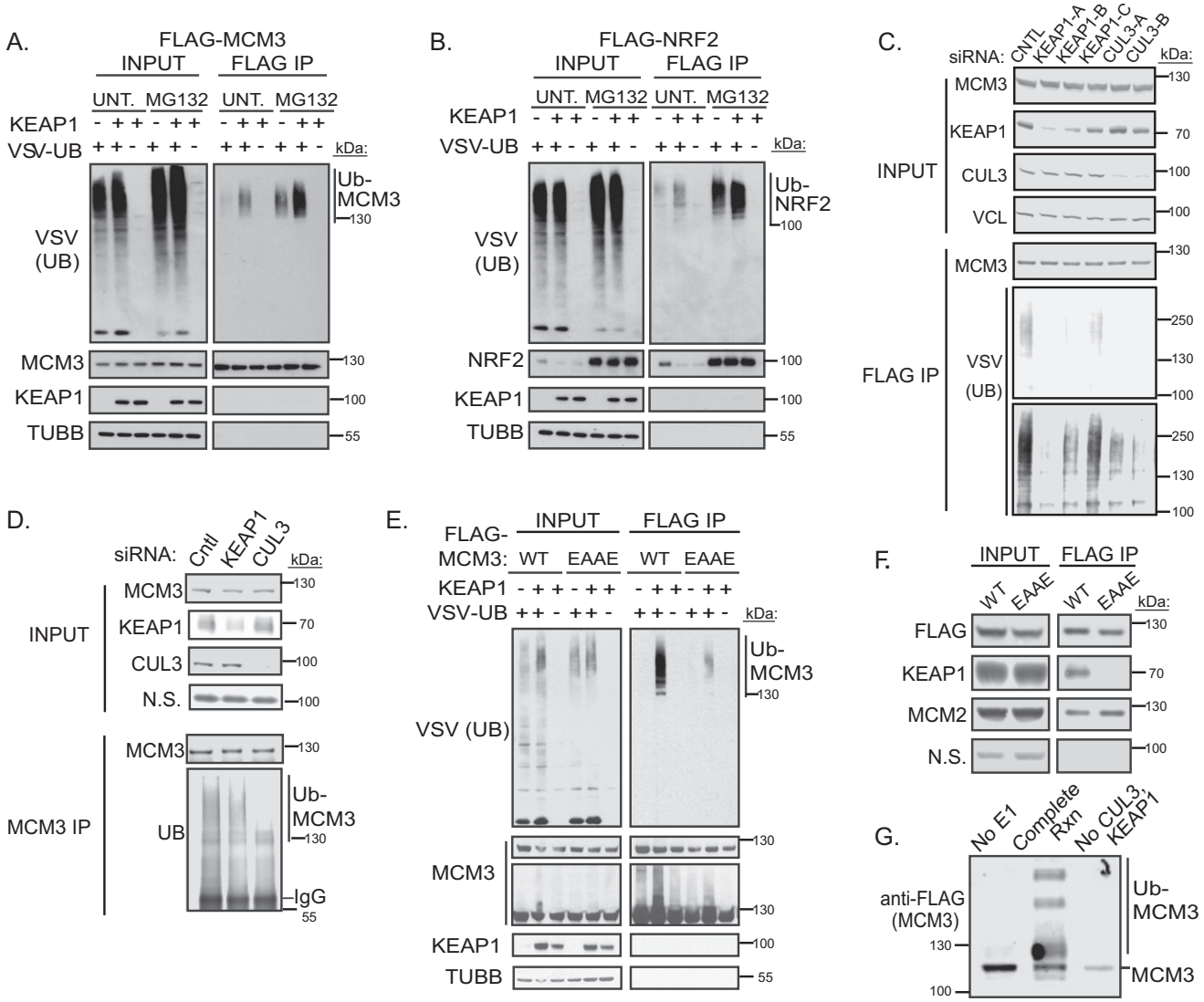

FIGURE 3. **MCM3 is a KEAP1-CUL3 substrate for ubiquitylation.** *A*, HEK293T cells were co-transfected with plasmids encoding SBPHA-KEAP1, FLAG-MCM3, and VSV-tagged ubiquitin (*UB*). Ubiquitylated MCM3 was detected by immunoblot analysis of immunopurified FLAG-MCM3 protein complexes. The IP was performed under near-denaturing conditions. *UNT*, untreated. *B*, HEK293T cells were co-transfected with plasmids encoding SBPHA-KEAP1, FLAG-NRF2 (positive control), and VSV-tagged ubiquitin. Ubiquitylated NRF2 was assessed by near-denaturing FLAG-NRF2 IP as in *A*. *C*, HEK293T cells stably expressing FLAG-MCM3 were transfected with control, KEAP1, or CUL3 siRNAs for 72 h, and the amount of ubiquitylated FLAG-MCM3 was determined as in *A*. *D*, ubiquitylation of endogenous MCM3 was determined by an anti-MCM3 IP after control (*Cntl*), KEAP1, or CUL3 siRNA transfection. *N.S.* is a nonspecific band shown as loading control (the nonspecific band was detected with anti-KEAP1 and was not affected by KEAP1 siRNA). *E*, HEK293T cells were transfected with plasmids encoding FLAG-MCM3 or FLAG-EAAE MCM3, and ubiquitylation was assayed as in *A*. *F*, HEK293T cells were transfected with plasmids encoding FLAG-MCM3 or FLAG-EAAE MCM3 and assessed for binding to KEAP1 by FLAG IP and Western blotting. *G*, *in vitro* ubiquitylation assay using KEAP1, CUL3-RBX1, UB, Ube1 (E1), UbcH5B (E2), and FLAG-MCM3. *No E1* and *No CUL3/KEAP1* served as negative controls. UB-MCM3 was detected by anti-FLAG (MCM3). These data are representative of two to five biological replicates of each (*A*–*G*). No CUL3/KEAP1 served as negative controls, complete reaction is denoted *complete Rxn*. *VCL*, vinculin.

that the KEAP1-CUL3 complex directly ubiquitylates MCM3. To confirm this, an *in vitro* ubiquitylation assay was performed. The KEAP1-CUL3-RBX1 complex was sufficient to ubiquitylate MCM3 (Fig. 3*G*).

To identify the sites of ubiquitylation within MCM3, and specifically those that respond to KEAP1, we performed ubiquitin remnant profiling on immunopurified MCM3 complexes from control cells or cells overexpressing KEAP1. Specifically, tryptic peptides from FLAG-MCM3 complexes were subjected to ubiquitin remnant IP followed by LC/MS-MS. This method uses an antibody specific for the ubiquitin remnant left on the ubiquitylated lysine following tryptic digestion. The results (Fig. 4*A*) further support our Western blotting data that KEAP1 indeed ubiquitylates MCM3. Using a 3-fold arbitrary threshold, six lysine residues were identified as responsive to KEAP1-dependent ubiquitylation: Lys-229, Lys-270, Lys-283, Lys-351, Lys-435, and Lys-748 (Fig. 4*A*). Of the ubiquitylated lysines mapped, Lys-435 showed the greatest -fold increase by KEAP1. This site was also found to be differentially ubiquitylated in an unbiased screen for cullin ring ligase substrates (57). To visualize these lysines on the structure of the MCM2–7 complex, we used protein structural modeling. Human MCM3 was threaded around a homologous archaeal MCM protein (58) and superimposed over a published model of the yeast MCM2–7 hetero-

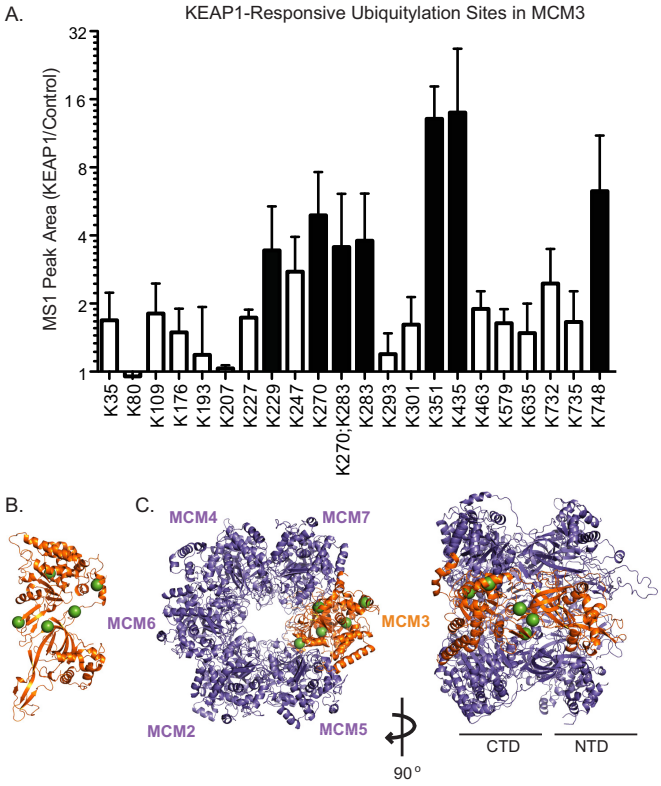

FIGURE 4. **Mapping the KEAP1-dependent ubiquitylation sites in MCM3.** *A*, HEK293T cells were transfected with plasmids encoding FLAG-MCM3 with or without the SBPHA-KEAP1 plasmid, and a near-denaturing FLAG IP was performed as in Fig. 3. A tryptic digest and ubiquitin remnant IP were then performed, followed by LC/MS-MS on the resultant peptides. Ubiquitylated peptides of MCM3 detected are plotted as mean ± S.E. MS1 peak areas of three biological replicate experiments. *Black columns* are lysine residues that increased beyond an arbitrary threshold of 3-fold increase in the presence of SBPHA-KEAP1 (supplemental Table S3). *B*, protein structural modeling of human MCM3 (Uniprot code P25205-1) threaded around an archaeal MCM structure (PDB code 3F9V). The KEAP1-modified lysines detected in *A* are shown as *green spheres*. *C*, protein structural modeling of human MCM3 from *B* superimposed over the published model of the yeast MCM2–7 complex (59). The KEAP1-modified lysines detected in *A* are shown as *green spheres*. A top-down view (*left panel*) and side view (*right panel*) are shown. *CTD*, C-terminal domain; *NTD*, N-terminal domain.

hexamer (59). The lysines observed to be most ubiquitylated in response to ectopic KEAP1 were found to be on predicted exposed surfaces of the C-terminal domain in MCM3 (Fig. 4, *B* and *C*).

KEAP1 Does Not Regulate MCM3 Levels, Subcellular Localization, or MCM2–7 Complex Formation—After identifying MCM3 as a novel KEAP1 substrate, we sought to determine the function of this ubiquitylation. First, we tested whether KEAP1 targets MCM3 for proteasome-mediated degradation as it does its well known substrate NRF2. KEAP1 manipulation did not affect steady-state levels of total cellular MCM3. Specifically, KEAP1 knockdown, deletion, overexpression, or chemical antagonism caused no changes in total MCM3 protein levels, whereas all of these perturbations affected NRF2 levels (Fig. 5, *A–D*). Attempts to determine whether KEAP1 loss affects MCM3 half-life were hampered by the extremely long MCM3 half-life. A very long (30-h) chase with the protein synthesis inhibitor cycloheximide did not yield an appreciable change in MCM3 levels (Fig. 5*F*), in agreement with a report that showed that the MCM complex had a half-life of ~24 h *in vivo* (60). Treatment with the proteasome inhibitor bortezomib also did not stabilize MCM3 over the course of 8 h, in agreement with KEAP1-CUL3-RBX1 not targeting MCM3 for proteasome-mediated degradation (Fig. 5*D*). Similarly, treatment with the lysosomal inhibitor chloroquine did not stabilize MCM3 over an 8-h time course, supporting the conclusion that the KEAP1-CUL3-RBX1 ligase is not targeting MCM3 for lysosome-mediated degradation (Fig. 5*E*).

Next we tested whether KEAP1 could be ubiquitylating MCM3 to affect its subcellular localization. Using immunofluorescence in HEK293T cells transiently transfected with KEAP1, we found no difference in the localization of endogenous MCM3, which remains largely diffuse in the nucleus (Fig. 5*H*, compare cells expressing KEAP1 in *red* to those not expressing). We also expressed increasing amounts of exogenous KEAP1 and assayed the amounts of MCM3 in the nuclear and cytoplasmic compartments and found no difference in the amount of MCM3 in either compartment, suggesting that KEAP1 does not regulate total MCM3 subcellular localization (Fig. 5*G*).

The ability of MCM3 to associate with the other members of the MCM2–7 heterohexamer was evaluated by immunoprecipitating either WT FLAG-MCM3 or the KEAP1-deficient binding mutant (FLAG-MCM3 EAAE) and probing with anti-MCM2. A comparable amount of MCM2 associated with both forms of MCM3, suggesting that KEAP1 binding and ubiquitylation do not regulate MCM3 incorporation into the MCM2–7 hexamer (Fig. 3*F*). Furthermore, MCM3 was associated with the other MCM proteins at similar levels in the presence or absence of KEAP1 siRNA knockdown (data not shown).

KEAP1-dependent Ubiquitylation Is Not Responsive to Treatment with DNA-damaging Agents, ROS Mimetics, or Autophagy—As DNA damage by etoposide was recently reported to lead to increased phosphorylation and ubiquitylation of a number of sites in subunits of the MCM2–7 complex (61), including three ubiquitylation sites within MCM3, we examined whether KEAP1 could be one of the E3 ligases that ubiquitylate MCM3 in response to DNA damage. We found, however, that overnight treatment with a panel of DNA-damaging agents (etoposide, gemcitabine, and 4-Nitroquinoline 1-oxide (4NQO)) did not strongly affect the MCM3-KEAP1 interaction (Fig. 6*A*) or KEAP1-dependent ubiquitylation of MCM3 but did activate phospho-Chk1, a marker of DNA damage (Fig. 6*B*). These data suggest that KEAP1 is not the ligase modifying MCM3 in response to etoposide-mediated DNA damage.

The ability of KEAP1 to act an as efficient substrate adaptor for NRF2, its well known substrate, relies on the redox state of the cell because, during oxidative stress, KEAP1 undergoes electrophilic attack by ROS and is placed in a conformation no longer favorable to target NRF2 (3, 6, 11, 12, 62–64). To test whether MCM3 is also a ROS-dependent substrate of KEAP1, we employed surrogate compounds (sulforaphane and *tert*-butylhydroquinone (tBHQ)) that mimic ROS by attacking the reactive cysteines within KEAP1. These drugs are widely used as NRF2 agonists, although whether these inhibit NRF2 ubiquitylation or block release of ubiquitylated NRF2 is debated. Here we find that treatment with these compounds stabilizes

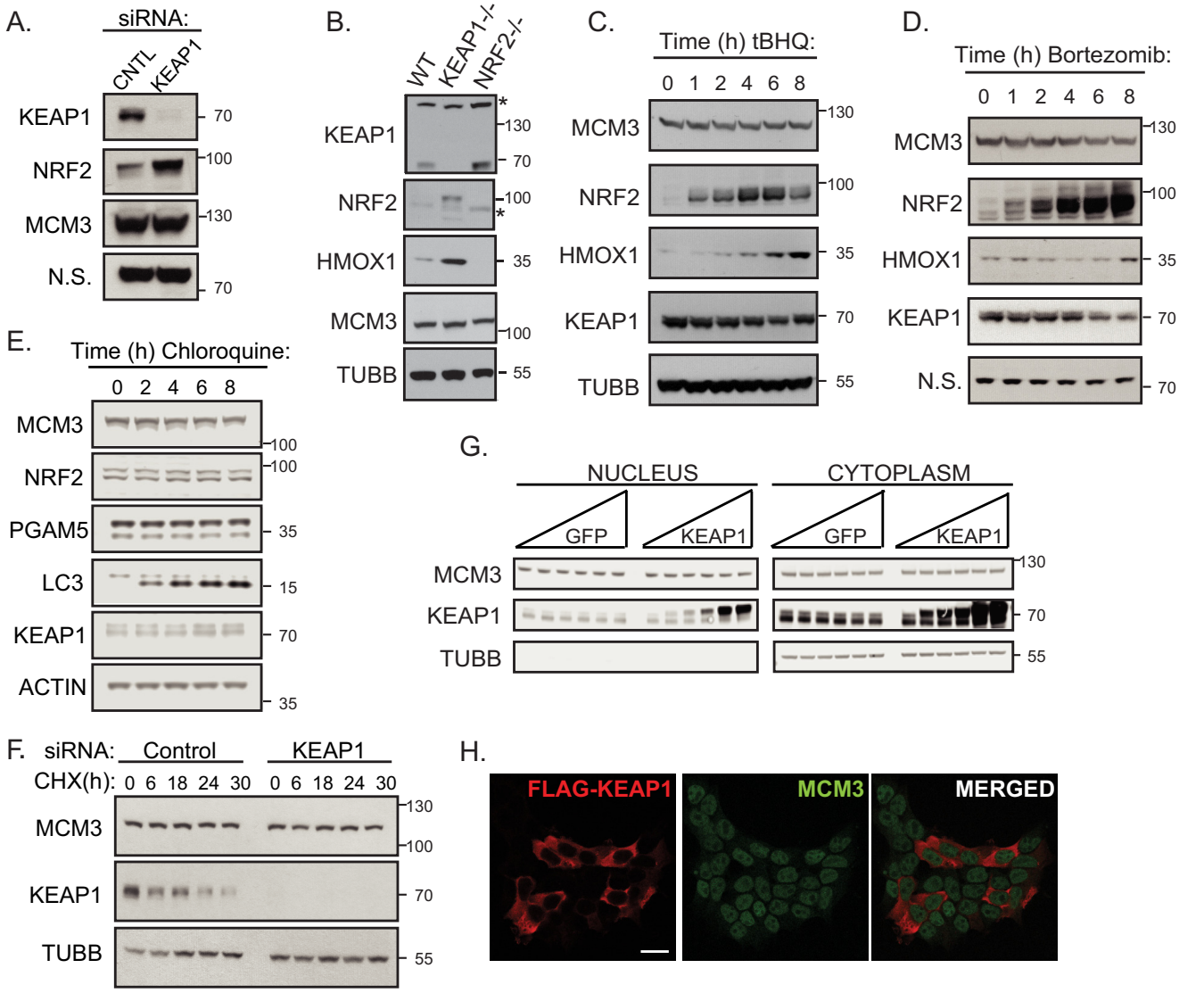

FIGURE 5. **MCM3 levels and subcellular localization are not regulated by KEAP1.** *A*, HEK293T cells were transfected with control or KEAP1 siRNA (20 nM, 72 h), lysed, and probed for KEAP1, NRF2, and MCM3 protein levels. *CNTL*, control. *N.S.* is a nonspecific band that served as a loading control (detected with anti-KEAP1 and was not changed by KEAP1 siRNA). *B*, WT, KEAP1$^{-/-}$, or NRF$^{-/-}$ MEFs were lysed and probed for KEAP1, NRF2, MCM3, and HMOX1 protein levels by Western blotting. Beta tubulin (*TUBB*) serves as a loading control. *C*, HEK293T cells were treated with the KEAP1 antagonist/ROS mimetic compound tBHQ at 50 μM for 0–8 h. Whole cell lysates were subjected to Western blotting for MCM3, KEAP1, NRF2 (positive control), HMOX1, and TUBB as a loading control. *D*, HEK293T cells were treated with 40 nM bortezomib (proteasome inhibitor) for 0–8 h before Western blotting. *E*, HEK293T cells were treated with the lysosomal degradation inhibitor chloroquine at 100 μM for 0–8 h. Whole cell lysates were subjected to Western blotting for MCM3, KEAP1, NRF2, LC3 (positive control), and Actin as a loading control. *F*, HEK293T cells were transfected with control or KEAP1 siRNA for 48 h, followed by a 30 h cycloheximide (*CHX*) treatment (10 μg/ml), and lysates were probed for MCM3, TUBB, and KEAP1 protein levels. *G*, HEK293T cells were transfected with increasing amounts of SBPHA-GFP or SBPHA-KEAP1 plasmid, lysed by fractionation into nuclei and cytoplasm, and blots were probed for MCM3, KEAP1, and loading and fractionation controls. *H*, HEK293T cells were transfected with FLAG-KEAP1 plasmid and stained for endogenous MCM3 and anti-FLAG to determine MCM3 localization in the presence or absence of KEAP1. Images were acquired on a confocal microscope. *Scale bar* = 20 μm. Each experiment (*A*–*H*) is representative of two to three biological replicates.

NRF2 but does not ablate KEAP1-dependent ubiquitylation of either NRF2 or MCM3 (Fig. 6, *C* and *D*). Together, these data suggest that the ubiquitylation of MCM3, like NRF2, is not inhibited by sulforaphane or tBHQ.

As MCM3, along with other important DNA replication factors, was recently reported to undergo autophagy-mediated degradation, we tested whether KEAP1 could be ubiquitylating MCM3 to target it for lysosomal degradation (65). We found that treatment with a lysosome-mediated degradation inhibitor (chloroquine, 100 μM for 8 h) or an autophagy activator (rapamycin, 10 μM for 8 h) did not affect KEAP1-dependent ubiquitylation of MCM3 but did augment LC3 I/II conversion, a marker of autophagy (Fig. 6*E*). These data suggest that KEAP1 is not targeting MCM3 for autophagy-mediated degradation.

KEAP1 Associates with Chromatin in a Cell Cycle-dependent Fashion—Our detection of KEAP1-MCM3 association in the nuclei of actively proliferating cells suggested that KEAP1 may associate with MCM3 during a normal cell cycle. MCM3 is chromatin-loaded as part of the MCM2–7 complex during G_1 phase and unloaded as DNA replication completes throughout S phase. To examine whether KEAP1 associates with chromatin in a cell cycle-dependent fashion, HeLa cells were synchro-

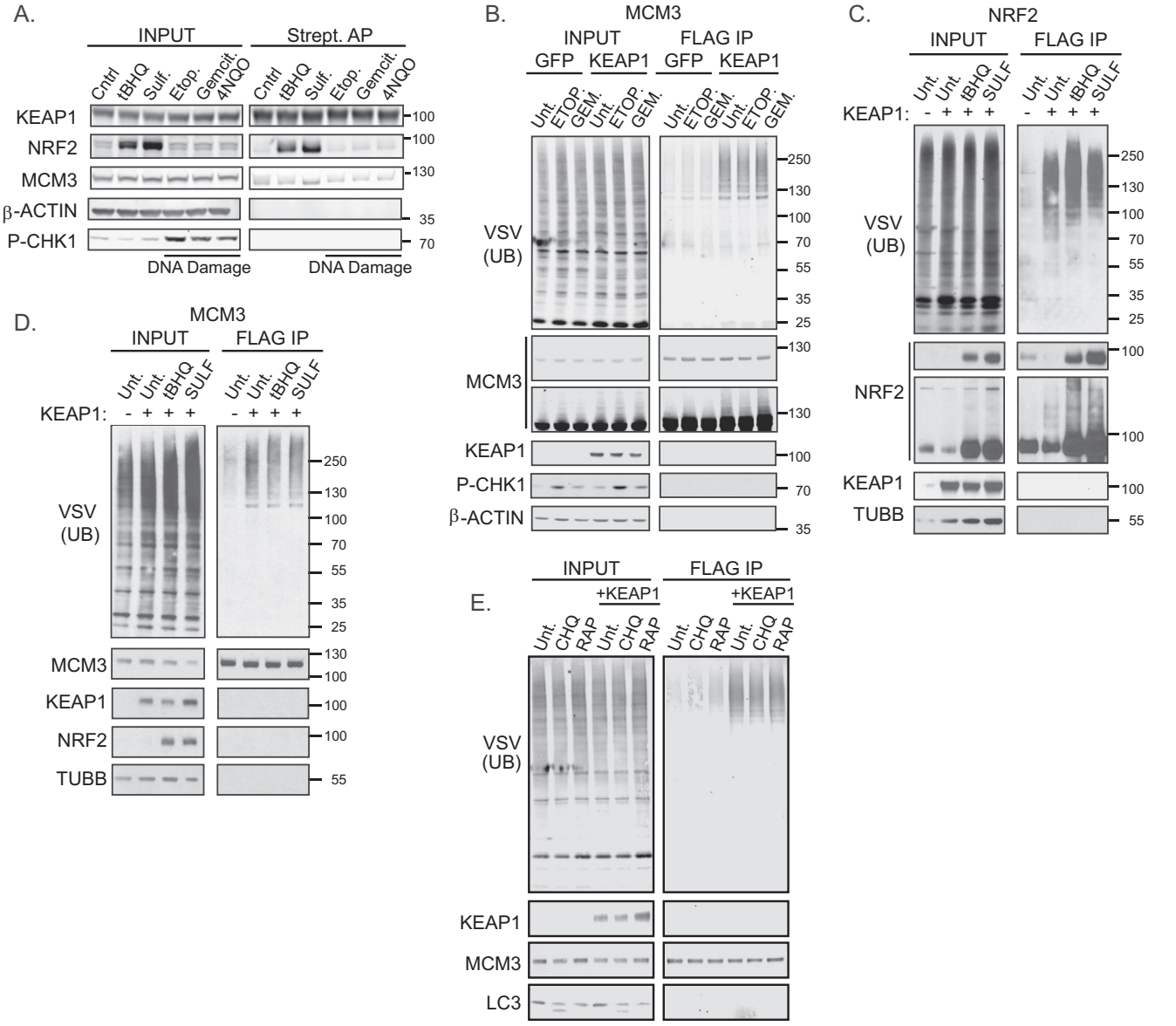

FIGURE 6. **MCM3 ubiquitylation by KEAP1 is not affected by DNA damage, ROS mimetics, or autophagy.** *A*, HEK293T cells stably expressing SBPHA-KEAP1 were treated overnight with a panel of DNA-damaging agents (etoposide (*Etop*), 20 μM; gemcitabine (*Gemcit*), 1 μM; 4NQO, 100 nM) or KEAP1 antagonists (tBHQ, 50 μM; sulforaphane (*Sulf*), 20 μM). Western blotting analysis of KEAP1 affinity-purified protein complexes are shown. Phospho-Chk1 serves as a marker of DNA damage. *Strept*, streptavidin; *Cntl*, control. *B*, HEK293T cells were transfected with plasmids encoding FLAG-MCM3 and VSV-ubiquitin (*UB*) with or without KEAP1 and were treated with DNA-damaging agents as in *A*. *C*, MCM3 ubiquitylation assays were performed as in Fig. 3. *Unt*, untreated. *D*, FLAG-NRF2 and VSV-UB with or without KEAP1 were transfected into HEK293T cells and treated with or without ROS mimetics/KEAP1 antagonists for 6 h as indicated (tBHQ, 50 μM; sulforaphane, 20 μM). Ubiquitylation of NRF2 was assayed as in Fig. 3. *E*, HEK293T were transfected with plasmids encoding FLAG-MCM3 and VSV-UB with or without KEAP1 and treated with or without ROS mimetics/KEAP1 antagonists as in *C*. MCM3 ubiquitylation was assayed as in Fig. 3. *E*, HEK293T cells were transfected with plasmids encoding FLAG-MCM3 and VSV-UB with or without KEAP1 and treated with or without chloroquine (lysosomal degradation inhibitor; 100 μM) or rapamycin (autophagy inducer, 10 μM) for 6 h. MCM3 ubiquitylation was assayed as in Fig. 3. LC3 I-II conversion served as a control for treatment. Each experiment (*A*–*E*) is representative of two to three biological replicates.

nized, and lysates were collected during G_1 and early S phase. The lysates were fractionated into chromatin and soluble fractions and immunoblotted for KEAP1, MCM3, and fractionation and loading controls. Strikingly, we found that KEAP1 loaded onto chromatin during G_1 phase as MCM3 did (Fig. 7*A*, loading is seen at the 4- to 10-h time points, chromatin fraction). To investigate when KEAP1 also unloads from the chromatin, HeLa cells were synchronized in early S phase, and lysates were collected from S to M phase. These lysates were fractionated into chromatin and whole cell fractions and probed for KEAP1, MCM3, and fractionation and loading controls. KEAP1 unloaded in G_2 phase, similar to MCM3, but the unloading of KEAP1 was slightly behind that of MCM3 (Fig. 7*B*, unloading is seen at the 6- to 10-h time points, chromatin fraction). Thus, KEAP1 associates with DNA in a cell cycle-dependent fashion, and KEAP1 is at the right place at the right time during the cell cycle to regulate the MCM complex.

In an asynchronous population, KEAP1 bound MCM3 predominantly in the soluble fraction with a weaker association on chromatin (Fig. 7*C*). This observation is consistent with the fact that most of the cellular MCM is soluble, and only a fraction is chromatin-loaded. To test where in the cell this KEAP1-depen-

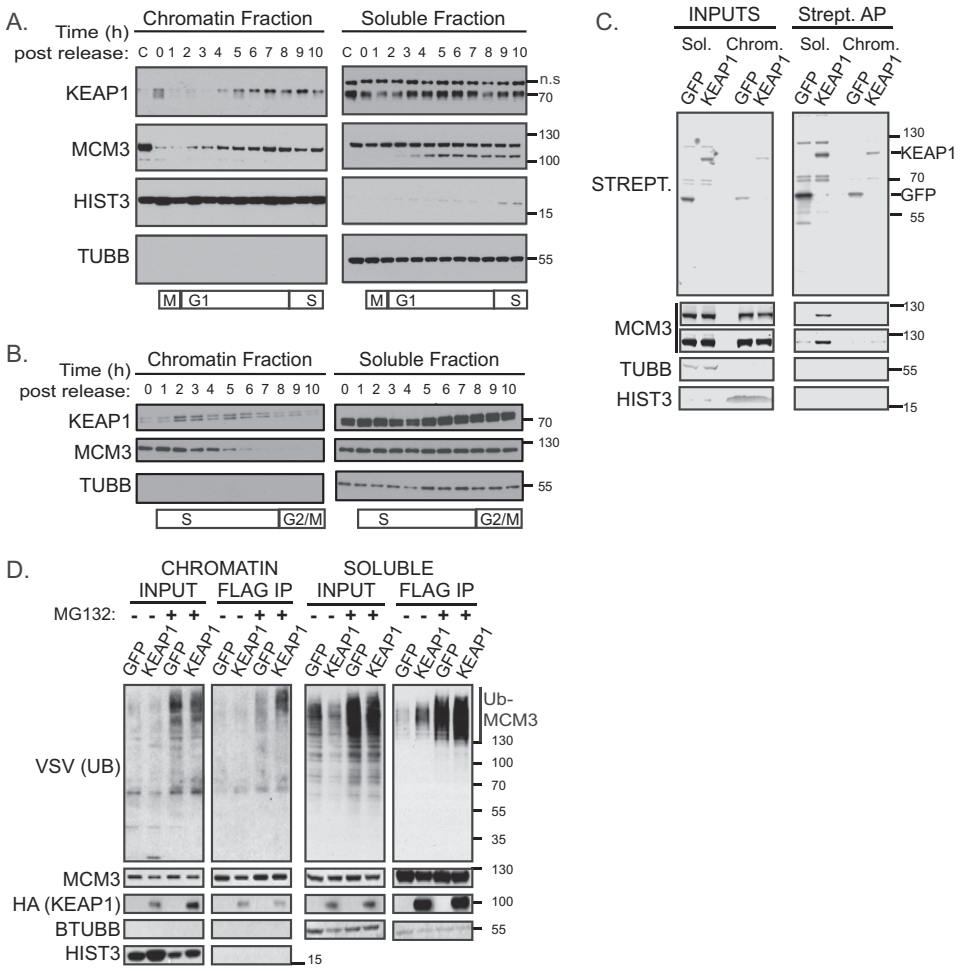

FIGURE 7. **KEAP1 associates with chromatin.** *A*, HeLa cells were transfected with control or KEAP1 siRNA and synchronized by double thymidine-nocodazole block. Lysates were collected during G_1 and S phases, separated into soluble and chromatin fractions, and probed for KEAP1, MCM3, and loading and fractionation controls (*C*). *B*, HeLa cells were transfected as in *A*, synchronized by double thymidine block, collected during S and G_2 phases, fractionated, and blotted as in *A*. *C*, HEK293T cells stably expressing BirA*-KEAP1 or BirA*-GFP were separated into chromatin (*Chrom*) and soluble (*Sol*) fractions, and the amount of MCM3 biotinylated by KEAP1 in each fraction was assessed by streptavidin (*Strept*) AP. *D*, HEK293T cells were transfected with the indicated plasmids and separated into chromatin and soluble fractions. Ubiquitylated MCM3 in each fraction was evaluated by IP/Western blotting. Each experiment is representative of two to three biological replicates. *TUBB*, beta tubulin; *n.s.*, non-specific band.

dent ubiquitylation occurs, cells expressing FLAG-MCM3 and either GFP or KEAP1 were fractionated into chromatin and soluble fractions, subjected to FLAG (MCM3) IPs in both fractions, and probed by Western blotting for ubiquitin on MCM3. Most ubiquitylation of MCM3 by KEAP1 was seen in the soluble fraction. Ubiquitylation of MCM3 in the chromatin-bound fraction was detectable, although only during proteasome inhibition (Fig. 7*D*). Therefore, KEAP1-dependent ubiquitylation of MCM3 occurs in both the chromatin and soluble fractions.

Discussion

Through its ubiquitin ligase activity, KEAP1 serves as a sensor and molecular switch for the cellular response to oxidative stress. Here we provide data that support the emerging concept of NRF2-independent functions for KEAP1. To date, in addition to NRF2 signaling and the coordinated antioxidant response, KEAP1 has been shown to regulate NF-κB signaling through its degradation of IKBKB to target the mitochondrial membrane phosphatase PGAM5 for proteasome-mediated degradation and to regulate DNA break repair through degradation-independent ubiquitylation of PALB2 (21–23). Our analyses here establish a fourth NRF2-independent function for KEAP1 and raise the additional possibility that KEAP1 regulates cell cycle progression and/or genome stability through ubiquitylation of MCM3.

Here we focused on a biochemical assessment of KEAP1 substrates in general and on defining MCM3 as a KEAP1 substrate in particular. Our future studies will delve into the role of KEAP1 in MCM3 function or dynamics. Our present data suggest that KEAP1 interacts with MCM3 when it is in the MCM2–7 hexameric complex. We detected KEAP1 in MCM2 immunoprecipitates, and, further, we observed biotinylation of MCM2 by the BirA*-tagged KEAP1. Together, these data suggest that KEAP1 interacts with the full MCM2–7 hexamer (*e.g.* Fig. 2*C*). Moreover, we detected KEAP1-mediated MCM3 ubiquitylation in both the soluble and chromatin-bound fractions (Fig. 7*D*). The association of KEAP1 with chromatin during S phase in a pattern that closely follows MCM loading and unloading is also consistent with KEAP1 associating with the MCM complex rather than monomeric MCM3 because only

the MCM complex is loaded for replication and not individual subunits (66). We thus favor the notion that KEAP1 impacts the replication function of the MCM complex, although we cannot yet rule out KEAP1 involvement in a novel non-replication role for MCM3, as has been reported for other individual MCM subunits (67, 68).

The high-affinity KEAP1-targeting motif (ETGE) is uniquely found in MCM3 and not in the other five MCM subunits, suggesting that MCM3 is at least one direct point of contact between the MCM complex and KEAP1. MCM4 contains the lower-affinity DLG binding motif for KEAP1, raising the possibility for a second point of contact. All six subunits of the human MCM2–7 heterohexamer have been reported to be ubiquitylated in cells (69). It is thus possible that KEAP1 ubiquitylates additional MCM proteins. Based on the *S. cerevisiae* and *Drosophila melanogaster* MCM complexes, we presume that human MCM3 is adjacent to both MCM5 and MCM7 in the hexamer (70, 71). MCM5 constitutes one side of the MCM2/5 "gate" where the MCM ring opens to allow double-stranded DNA to pass during MCM loading in G_1 phase (72, 73). KEAP1 could modulate MCM loading by regulating conformational changes at the MCM2/5 interface. MCM3 is the subunit that directly contacts the helicase activator complex GINS, which only associates with MCM during helicase activation and fork progression (71). KEAP1-mediated MCM3 ubiquitylation could impact helicase activation either globally or at a subset of origins. Interestingly, polyubiquitylation of the MCM7 subunit in both *S. cerevisiae* and *X. laevis* is associated with replication termination and MCM unloading (49, 50, 52) but not changes in MCM7 stability. The KEAP1 interaction with MCM3 could also impact MCM unloading. KEAP1 could thus link ROS sensing to the control of MCM chromatin loading, to activation of MCM-dependent DNA unwinding, or to MCM unloading during S phase as a means to preserve DNA integrity and genome stability.

Human MCM complexes undergo cell cycle-dependent phosphorylation and sumoylation (46), and it is certainly possible that additional E3 ubiquitin ligases participate with KEAP1 in MCM control. Nonetheless, KEAP1 is clearly the major MCM3 E3 ubiquitin ligase in actively proliferating cells (Fig. 3). Our data so far suggest that KEAP1 binds and ubiquitylates only a subset of the total MCM3 molecules and likely regulates their activity through altering MCM2–7 protein-protein interactions or helicase activity. Future work will explore not only the molecular consequences of KEAP1-mediated MCM ubiquitylation but also under what cellular circumstances KEAP1 may be stimulated to ubiquitylate MCM3. Our discovery that KEAP1 associates with chromatin during S phase may reflect a novel nuclear role for KEAP1 in monitoring replication fork progression and perhaps coordinating origin firing or replisome activity with cellular redox state. If so, then the KEAP1-MCM interaction represents a novel, nuclear role for KEAP1 outside of NRF2 regulation, emphasizing the breadth of KEAP1-regulated cellular events.

We have previously defined a static KEAP1 protein interaction network and demonstrated that it is enriched for proteins containing the KEAP1 binding motif, E(T/S)GE (19, 20). Although the ETGE motif in NRF2 has been established as a KEAP1 degron therein, and several ETGE-containing proteins have been shown to activate NRF2 through competitive binding to KEAP1 (74, 75), the function of the interactions between KEAP1 and these other E(T/S)GE-containing proteins remained largely unknown. In this study, we have combined PAC proteomics to capture substrates and annotated them against what we identified in our prior studies to be high-confidence KEAP1 interactors. Our data suggest that, in addition to MCM3, which we validated as a KEAP1-CUL3-RBX1 substrate here, we may have also discovered NRF1 as a novel KEAP1 substrate. NRF1 has been shown previously to bind KEAP1, but KEAP1 was shown not to be responsible for targeting NRF1 to the endoplasmic reticulum membrane or regulating an artificial reporter of NRF1-driven transcription (54, 55). To the best of our knowledge, our study is the first report that NRF1 is a putative KEAP1 substrate for proteasome-mediated degradation. We observe NRF1 accumulating with proteasome inhibition in both whole cell lysates and in the KEAP1 complex by both AP/MS and AP-Western blotting. In-cell and *in vitro* ubiquitylation assays will be important to confirm the substrate status of NRF1. Our findings neither confirm nor rule out whether MAD2L1, SLK, DPP3, TSC22D4, FAM117B, or other ETGE-containing KEAP1 interactors are *bona fide* substrates. Because we and others have now demonstrated that KEAP1-CUL3-RBX1 substrates may not be turned over by the proteasome (23), the substrate status of each of these interactors will need to be evaluated individually.

Here we broadly defined two classes of KEAP1 substrates: class I, comprised of NRF2 and, potentially, NRF1 and IKBKB, and class II, comprised of PGAM5, MCM3, and, potentially, PALB2, MAD2L1, and SLK (although not detected in our MS data, IKBKB and PALB2 have been validated by others in the field). These classes of substrates can likely be further characterized by whether or not the KEAP1 complex targets them for degradation and whether that degradation occurs via the proteasome or the lysosome. Additionally, the presence of both the DLG and ETGE motifs in the rapidly degraded class I substrates (NRF2, IKBKB, and NRF1) suggest that KEAP1-CUL3-RBX1 substrate dynamics may be governed by the number and/or types of degrons within a given substrate. This pattern is in contrast to the class II substrates PGAM5, PALB2, and MCM3, which contain only the E(T/S)GE motif. These proteins are generally longer-lived than class I proteins, and their ubiquitylation by KEAP1 may be unrelated to their stability. Thus, whether a KEAP1-CUL3-RBX1 substrate is marked for degradation by ubiquitylation and the dynamics of that degradation may be in part dependent on the presence of a DLG motif. The stoichiometry of the class II substrates PGAM5, PALB2, and MCM3 within the KEAP1 complex is not known. Whether these may contain a second KEAP1 binding motif that acts similarly to the DLG and positions these substrates for ubiquitylation by the KEAP-CUL3-RBX1 machinery merits further study.

This work is important from a basic biology standpoint because little is known about NRF2-independent functions for this redox-sensitive E3 ligase. Additionally, this is clinically relevant because a more complete understanding of this pathway is essential to treating patients harboring KEAP1 mutations and to fully grasping the impact of chemically altering the activity or

substrate interface of KEAP1. Furthermore, this work provides a previously unappreciated link between KEAP1, genome stability, and cell cycle progression.

Experimental Procedures

Tissue Culture, Treatments, Transfections, and Small Interfering RNAs—HEK293T, HDF-Tert, and HeLa cells were obtained from the American Type Culture Collection. The cell lines were passaged for no more than 3 continuous months after resuscitation. HDF-Tert, HEK293T, and HeLa cells were grown in DMEM supplemented with 10% FBS and 1% penicillin/streptomycin in a 37 °C humidified incubator with 5% CO_2. Mouse embryonic fibroblasts (MEFs) were cultured in Iscove's modified Dulbecco's medium supplemented with 10% FBS and 1% penicillin/streptomycin. The KEAP1 and NRF2 knockout MEFs were kindly provided by Thomas Kensler and Nobunao Wakabayshi. Drugs used for cell treatments were acquired as follows: MG132 (Calbiochem), bortezomib (SelleckChem), *tert*-butylhydroquinone (Sigma), sulforaphane (Sigma), etoposide (Sigma), chloroquine (Sigma), and gemcitabine (Sigma). For transient transfections, cDNA expression constructs were transfected in HEK293T cells using Lipofectamine 2000 (Life Technologies) for 24 h before harvest. Transfection of siRNA (20 nM) in HEK293T cells was performed with Lipofectamine RNAiMAX (Life Technologies). Transfection of siRNA in HeLa cells was done with either Dharmafect (50 nM) or Lipofectamine RNAiMAX (20 nM). siRNA sequences were as follows: control, CGUACGCGGAAUACUUCGATT; KEAP1-A, GGGCGUGGCUGUCCUCAAU; KEAP1-B, CAUGUGAUUUAUUCUUGGAUACCUG; KEAP1-C, UGGCUGUCCUCAAUCGUCUCCUUUA; CUL3-A, GGUCUCCUGAAUACCUCUCAUUAUU; and CUL3-B, GAAUGUGGAUGUCAGUUCACGUCAA.

Immunoprecipitations, Affinity Pulldowns, and Western Blotting—These experiments were performed as described previously (74) with minor modifications. Briefly, for streptavidin and FLAG affinity and immune purification, cells were lysed in 0.1% Nonidet P-40 lysis buffer (10% glycerol, 50 mM Tris-HCl, 150 mM NaCl, 2 mM EDTA, 0.1% Nonidet P-40 supplemented with protease inhibitor mixture (Thermo Scientific) and phosphatase inhibitor (Thermo Scientific), 10 mM *N*-ethylmaleimide, and 250 units Benzonase (Sigma)) and then passed through a 26.5-gauge needle three times. The cell lysates were cleared by centrifugation and incubated with streptavidin resin (GE Healthcare) or FLAG resin (Sigma) before washing with lysis buffer and eluting with NuPAGE 4× SDS loading buffer (Life Technologies). For siRNA knockdown, HEK293T cells were transiently transfected and lysed in RIPA buffer (1% Nonidet P-40, 0.1% SDS, 0.25% sodium deoxycholate, 150 mM NaCl, 10% glycerol, 25 mM Tris, and 2 mM EDTA supplemented with protease inhibitor mixture, phosphatase inhibitor, and *N*-ethylmaleimide) 60–72 h post-transfection. For BirA* affinity purification, HEK293T cells were pretreated with 50 μM biotin for 2–4 h and lysed in supplemented RIPA buffer, and cleared lysates were subjected to streptavidin AP as above and eluted with a 1:1:1:1 mixture of 1 M DTT, 4× SDS loading buffer, 50 μM biotin, and RIPA buffer. For endogenous IP (Fig. 2, *B* and *C*), HEK293T cells were lysed in co-IP buffer (50 mM HEPES (pH 7.2), 33 mM potassium acetate, 1 mM $MgCl_2$, 1 mM ATP, 0.1% Nonidet P-40, 5 mM $CaCl_2$, and 10% glycerol with protease and phosphatase inhibitors), then treated with 10 units of S7 micrococcal nuclease (Roche), sonicated, and cleared by centrifugation. Samples were rotated with MCM2 antibody or control rabbit IgG, followed by rotation with protein A-Sepharose (Roche), and then washed three times with co-IP buffer and eluted with 2× SDS loading buffer, 5% 2-mercaptoethanol (Sigma), and boiling for 10 min. Lysates were resolved on 4–12% SDS-PAGE gradient gels (Invitrogen), transferred to nitrocellulose or PVDF membranes, and probed using the following antibodies: anti-MCM3 (Bethyl, A300-192A), anti-KEAP1 polyclonal (ProteinTech, Chicago IL), anti-FLAG M2 monoclonal (Sigma), anti-HA monoclonal (Roche), anti-MAD2L1 (Bethyl, Montgomery TX, A300-301A), anti-SLK (Bethyl, A300-499A), anti-β-actin polyclonal (Sigma, A2066), anti-β-tubulin monoclonal (Sigma, T7816), anti-DPP3 polyclonal (Abcam, Cambridge, MA, 97437), anti-GFP (Abcam, ab290), anti-NRF2 H300 polyclonal (Santa Cruz Biotechnology, Santa Cruz, CA), anti-PGAM5 polyclonal (Abcam, 126534), anti-NRF1 polyclonal (Santa Cruz Biotechnology, D5B10), anti-MCM2 polyclonal (Bethyl, A300-191A), anti-Pan MCM (a kind gift from D. MacAlpine, Duke University), and anti-VSV polyclonal (Bethyl, A190-131A). Biotinylated proteins associated with BirA* AP blots were detected using fluorescently labeled streptavidin (IRDye 680CW-LI-COR). Protein quantification was performed in the LI-COR imaging suite (Image Studio Lite), where all blots were determined to be in the linear range by the software.

Cell Fractionations and Cell Synchronization—HeLa cells were synchronized with a double thymidine block in early S phase by treatment with 2 mM thymidine (Sigma) for 18 h, washout for 9 h, and readdition of 2 mM thymidine for an additional 17 h. HeLa cells were synchronized in M phase by double thymidine/nocodazole block: first, the double thymidine block (as above, with 24 h of 2 mM thymidine, 6 h of release, and readdition of thymidine for 18 h), and then cells were released into fresh DMEM containing 100 ng/ml nocodazole for 8–12 h. In each case, cells were washed twice with warm medium and released into fresh DMEM. Chromatin fractionation was performed by gentle lysis with CSK buffer (0.5% Triton X-100, 300 mM sucrose, 10 mM PIPES, 100 mM NaCl, and 2 mM EDTA) supplemented with protease and phosphatase inhibitors for 20 min on ice. Lysates were centrifuged at 900 × *g* for 5 min at 4 °C to pellet the nuclei. Soluble fractions were transferred to new tubes. The nuclei were resuspended in CSK buffer containing 10 units DNase (RQ1, Promega) for 10 min at room temperature and pelleted at 900 × *g* for 5 min at 4 °C. The remaining nuclei were washed once with CSK buffer, and the first DNase digest and the wash were pooled. Nuclear proteins solubilized by DNase digest were the chromatin fraction.

Plasmids, Expression Vectors, and Site-directed Mutagenesis—Expression constructs in the SBPHA backbone were generated with standard PCR techniques as described previously (20). The expression constructs for MCM3 and NRF2 were obtained from Open Biosystems and cloned into a custom gateway lentiviral vector (pHAGE-CMV-FLAG-DEST). MCM3 and NRF2 were obtained as orfeome entry

clones and gateway-cloned into pHAGE-CMV-FLAG-DEST. The MCM3 EAAE alanine mutant was created using PCR-based mutagenesis (Q5 site-directed mutagenesis kit, New England Biolabs) and sequence-verified before use.

Cell-based Ubiquitylation Experiments—These experiments were performed as reported previously (20) with few modifications. Briefly, HEK293T cells were transfected with VSV-UB, FLAG-NRF2, or FLAG MCM3 and either SBPHA-KEAP1 or SBP-GFP as a control so that each condition received the same mass of DNA. The cells were lysed under near-denaturing conditions in 1% SDS lysis buffer (1% SDS, 150 mM NaCl, and 2 mM EDTA) and boiled at 90 °C for 10 min. SDS lysis buffer was diluted 1:10 in cold 0.5% Nonidet P-40 lysis buffer supplemented with protease, phosphatase, and deubiquitylase inhibitors, and the lysates were cleared by centrifugation. FLAG IPs were carried out by incubating lysates with FLAG resin for 1–4 h at 4 °C, followed by washing three times in lysis buffer and eluting with 4× SDS loading buffer and DTT.

In Vitro Ubiquitylation Experiments—For *in vitro* ubiquitylation studies, SBPHA-KEAP1 was generated using a TnT assay (Promega), and MCM3 was purified from HEK293T cells stably expressing FLAG-MCM3 using 1% Triton-X lysis buffer (as described above for immunoprecipitations but with 500 mM NaCl). For the *in vitro* ubiquitylation assay, KEAP1 was mixed with recombinant human E1 (Ube1, Boston Biochem), UbcH5B (E2, Boston Biochem), CUL3-RBX1 (co-expressed in *Escherichia coli* as GST-Rbx1 and His-CUL3 fusions and purified sequentially over HiTRAP nickel-nitrilotriacetic acid (GE Healthcare) and glutathione-Sepharose (GE Healthcare) and proteolytically cleaved off the resin using thrombin (Sigma), followed by size exclusion chromatography over a Superdex-200 16/60 column (GE Healthcare)), ubiquitin (Boston Biochem), and FLAG-tagged MCM3 in buffer containing 25 mM HEPES (pH 8.0), 5 mM $MgCl_2$, 2 mM DTT, and 4 mM ATP. Ubiquitylation was carried out for 20 min at 30 °C, and the products were analyzed by Western blotting with anti-FLAG antibody.

Protein Structural Modeling—The crystal structure of an archaeal MCM from *Sulfolobus solfataricus* (PDB code 4FDG) was identified as a template for predicting the atomic structure of human MCM3 by HHpred (PMID 15531603), and the homology model was generated using MODELLER PMID 25199792). In the structural model, 94 residues at the C terminus as well as the residues between 510–562 were omitted because of poor homology to the archaeal MCM. The MCM3 model was superimposed onto a published model of the MCM2–7 heterohexamer from yeast (59) using PyMOL (The PyMOL Molecular Graphics System, version 1.3, Schrödinger, LLC). PyMOL was used to prepare the images used in Fig. 4, *B* and *C*.

Affinity Purification and Mass Spectrometry—These experiments were performed as described previously (19, 74, 76) with minor modifications. Briefly, HEK293T cells (3–5 × 15-cm plates) stably expressing either FLAG-MCM3 or SBPHA-KEAP1 were lysed in 0.1% Nonidet P-40 lysis buffer for FLAG IP or streptavidin AP, respectively. Cell lysates were incubated, rotating with FLAG or streptavidin resin for 1 h at 4 °C, and then washed three times with lysis buffer. The precipitated proteins were then trypsinized (Promega) on beads at 37 °C overnight (12–18 h) using the FASP protein digestion kit (Protein Discovery). For the KEAP1 substrate-trapping experiment (Fig. 1, *A* and *B*), SBPHA-KEAP1-expressing HEK293T cells were grown in SILAC media (light, K_0R_0; heavy, K_6R_{10}) for at least 10 cell divisions prior to harvesting for lysis. Tryptic peptides were cleaned up using a C18 spin column (Thermo Scientific) and then separated by reverse-phase nano-HPLC using a nano-Aquity ultra performance liquid chromatography (UPLC) system (Waters Corp.). Chromatographic separation and mass spectrometry analysis of peptides from FLAG-MCM3 experiments (Fig. 2*A*) were performed using the same methods as in our previous work (76). Peptides from SBPHA-KEAP1 and ubiquitin remnant experiments were first trapped in a 2-cm trapping column (Acclaim® PepMap 100, C18 beads of 3.0-μm particle size, 100-Å pore size) and a 25-cm EASY-spray analytical column (75-μm inner diameter, C18 beads of 2.0-μm particle size, 100-Å pore size) at 35 °C. The flow rate was 250 nl/min over a gradient of 1% buffer B (0.1% formic acid in acetonitrile) to 30% buffer B in 180 min, and an in-line Orbitrap Elite mass spectrometer (Thermo Scientific) performed mass spectral analysis. The ion source was operated at 2.4–2.8 kV with the ion transfer tube temperature set at 300 °C. A full MS scan (300–2000 m/z) was acquired in Orbitrap with a 120,000 resolution setting, and data-dependent MS2 spectra were acquired in the linear ion trap by collision-induced dissociation using the 15 most intense ions. Precursor ions were selected based on charge states (^{3}+2) and intensity thresholds (above 1e5) from the full scan; dynamic exclusion (one repeat during 30 s, a 60-s exclusion time window) was also used. The polysiloxane lock mass of 445.120030 was used throughout spectral acquisition.

Protein Identification, Filtering, and Bioinformatics—For the MCM3 protein interaction network (Fig. 2*A*), the raw mass spectrometry data were searched with MaxQuant (1.5.2.6) along with an internal lab FLAG affinity purification mass spectrometry (APMS) dataset of an additional 17 baits and 35 experiments. The search parameters were as follows: specific tryptic digestion, up to two missed cleavages, a static carbamidomethyl cysteine modification, variable protein N-terminal acetylation, and variable methionine oxidation using the human UniProtKB/Swiss-Prot sequence database (release 2013_07). Proteins were then filtered for a 1% protein level false discovery rate (FDR). Filtering of false interactions was then accomplished using Spotlite (19), with a 10% FDR for the entire dataset, including the additional baits. These results were then imported into Cytoscape v3.2.1 for network visualization. The Spotlite results are provided in supplemental Table S2. For the SBPHA-KEAP1 SILAC experiments, the additional MaxQuant parameters were a variable Gly-Gly modification on lysines, and Lys-6 and Arg-10 heavy SILAC labels. The Maxquant results are provided in supplemental Table S1.

For ubiquitin remnant profiling, raw files were searched using Sorcerer™-SEQUEST® (build 5.0.1, Sage N Research) and the Transproteomic Pipeline (TPP v4.7.1). The search parameters used were a precursor mass between 400 and 4500 amu, a maximum of two missed cleavages, a precursor ion tolerance of 3 atomic mass unit (amu), accurate mass binning

within PeptideProphet, semitryptic digestion, a static carbamidomethyl cysteine modification (57.021465), and variable methionine oxidation (+15.99492), ubiquitylated lysine (114.042931), and serine, threonine and tyrosine (STY) phosphorylation (79.966331). A 1% peptide-level FDR was determined by PeptideProphet. The mass spectrometry proteomics data have been deposited in the ProteomeXchange Consortium via the PRIDE (77) partner repository with the dataset identifier PXD003929.

Ubiquitin Remnant Profiling—For mapping the ubiquitylated lysines within MCM3, immunoprecipitations for FLAG-MCM3 were done under near-denaturing conditions in the presence or absence of SBPHA-KEAP1. Then, the proteins were subject to tryptic digest and the peptides were flowed over beads conjugated to the ubiquitin remnant specific antibody (Cell Signaling) for 4 h at 4°C in IAP buffer supplied by the manufacturer. Beads were washed twice with IAP buffer and once with PBS. Peptides were eluted with 0.15% TFA for 5 min at room temperature and dried at room temperature by speed vacuuming. Peptides were shot in the mass spectrometer as described above. Ubiquitylated peptides identified by MS/MS were then quantified in Skyline v3.5. For each peptide, the MS1 intensity of its extracted ion chromatogram was integrated for each of 3 label-free replicate experiments (3 runs with KEAP1, 3 runs without KEAP1). Any peptide identified by MS/MS or which was aligned by *m*/*z*, retention time, and had an isotope dot product >.8 was included in the analysis. The mean total area of each MS1 belonging to a ubiquitylated MCM3 peptide was taken from the 3 replicate experiments and a ratio was created for the +KEAP1/-KEAP1 conditions. For any peptide found to be true in one condition, but that was missing in the other, the background at the same mass to charge window was quantified to calculate a-fold change. The complete results are provided in Table S3. The mass spectrometry proteomics data have been deposited to the ProteomeXchange Consortium via the PRIDE (77) partner repository with the dataset identifier PXD003929.

Immunostaining—These experiments were performed as reported previously with minor modifications (76). To determine the subcellular distribution of KEAP1 and MCM3 proteins, HEK293T cells stably expressing VENUS-KEAP1 were plated on 10 μg/ml fibronectin-coated coverslips in DMEM supplemented with 10% fetal bovine serum and subjected to staining. Cells were fixed in 4% paraformaldehyde in cytoskeletal buffer (5 mM PIPES (pH 6), 137 mM NaCl, 5 mM KCl, 1.1 mM Na_2HPO_4, 0.4 mM KH_2PO_4, 0.4 mM $MgCl_2$, 0.4 mM $NaHCO_3$, 2 mM EGTA, and 50 mM glucose) for 15 min and permeabilized with 0.1% Triton X-100/PBS solution for 5 min. After blocking with 1% BSA/PBS, cells were incubated overnight with a rabbit polyclonal antibody against MCM3 (Bethyl, 1:250 dilution), followed by incubation with TRITC-conjugated donkey secondary antibody (1:300 dilution) against rabbit IgG. Coverslips were mounted to slides using the Prolong Gold antifade reagent (Invitrogen/Molecular Probes), and images were acquired using a Zeiss LSM710 confocal laser-scanning microscope equipped with ×40/1.3 Oil Plan Neo and ×63/1.4 Oil Plan Apo objective lenses.

Proximity Ligation Assays—For detection of KEAP1 and MCM3 interactions, proximity ligation was performed with the Duolink II proximity ligation assay kit according to the protocol of the manufacturer (Sigma, DUO092101). Briefly, HEK293T cells stably expressing VENUS-KEAP1 were plated, fixed, and permeabilized as described above. Next, cells were incubated in blocking solution in a humidified chamber at 37 °C for 30 min, followed by overnight co-incubation with rabbit polyclonal antibodies against MCM3 (Bethyl, 1:250) and mouse monoclonal antibody against KEAP1 (Origene, 1:100) in antibody diluent solution at 4 °C. Cells were washed in buffer A and incubated with PLA probes (PLA probe minus and plus in antibody diluent, 1:5 dilution) for 1 h at 37 °C, washed in buffer A, and incubated with ligation solution (1:5 dilution of ligation buffer and 1:40 dilution of ligase in pure water) for 30 min at 37 °C. After ligation, cell were washed in buffer A and subjected to amplification with Detection Reagents Red from (1:5 dilution amplification stock and 1:80 dilution of polymerase in water) for 100 min at 37 °C. Amplified samples were washed in buffer B and then mounted with Duolink II mounting medium with DAPI. Confocal Z-stack images were acquired using a Zeiss LSM710 spectral confocal laser-scanning microscope equipped with a ×63/1.42 Oil PlanApo objective lens. ImageJ software was used to process the images to a two-dimensional illustration of all dots in each cell.

Author Contributions—K. M. M. designed and performed the majority of the experiments, analyzed and interpreted the experimental results, and provided the manuscript draft. J. P. M. performed cell synchronization and endogenous co-immunoprecipitation experiments and edited the manuscript. P. F. S. performed immunofluorescence and PLA experiments and edited the manuscript. T. Y. T. and D. G. ran the LC/MS-MS instrument for the MS experiments. D. G. also contributed to MS data analysis and made the protein interaction networks. T. Y. T. also performed a subset of the KEAP1 affinity purifications and edited the manuscript. J. S. H. and E. W. C. generated proteins for the *in vitro* ubiquitylation assays and edited the manuscript. T. M. J. made the PyMOL models and edited the manuscript. C. V. conceived several experiments, advised on experimental design, and provided data interpretation. M. B. M. and J. G. C. edited the manuscript, analyzed and interpreted data, and advised on project maturation. All authors have reviewed the results and approved the final version of the manuscript.

Acknowledgments—We acknowledge the University of North Carolina R. L. Juliano Structural Bioinformatics Core Facility, particularly Brenda Temple, for structural modeling of human MCM3 and Christopher Brandl from the University of Western Ontario, who provided PyMOL builds of the yeast MCM complex. We thank David MacAlpine of Duke University for the gift of the pan-MCM antibody and members of the Major, Cook, Vaziri, and Emanuele laboratories for technical support, protocols, reagents, and thoughtful discussion related to this project. Additionally, we thank Michael Emanuele for critical reading of this manuscript.

References

1. Kobayashi, A., Ohta, T., and Yamamoto, M. (2004) Unique function of the Nrf2-Keap1 pathway in the inducible expression of antioxidant and detoxifying enzymes. *Methods Enzymol.* **378,** 273–286

2. Furukawa, M., and Xiong, Y. (2005) BTB protein Keap1 targets antioxidant transcription factor Nrf2 for ubiquitination by the Cullin 3-Roc1 ligase. *Mol. Cell. Biol.* **25,** 162–171
3. Zhang, D. D., Lo, S. C., Cross, J. V., Templeton, D. J., and Hannink, M. (2004) Keap1 is a redox-regulated substrate adaptor protein for a Cul3-dependent ubiquitin ligase complex. *Mol. Cell. Biol.* **24,** 10941–10953
4. Baird, L., and Dinkova-Kostova, A. T. (2013) Diffusion dynamics of the Keap1-Cullin3 interaction in single live cells. *Biochem. Biophys. Res. Commun.* **433,** 58–65
5. Jiang, Z. Y., Chu, H. X., Xi, M. Y., Yang, T. T., Jia, J. M., Huang, J. J., Guo, X. K., Zhang, X. J., You, Q. D., and Sun, H. P. (2013) Insight into the intermolecular recognition mechanism between Keap1 and IKKβ combining homology modelling, protein-protein docking, molecular dynamics simulations and virtual alanine mutation. *PLoS ONE* **8,** e75076
6. Zhang, D. D., and Hannink, M. (2003) Distinct cysteine residues in Keap1 are required for Keap1-dependent ubiquitination of Nrf2 and for stabilization of Nrf2 by chemopreventive agents and oxidative stress. *Mol. Cell. Biol.* **23,** 8137–8151
7. Nguyen, T., Sherratt, P. J., Huang, H. C., Yang, C. S., and Pickett, C. B. (2003) Increased protein stability as a mechanism that enhances Nrf2-mediated transcriptional activation of the antioxidant response element: degradation of Nrf2 by the 26S proteasome. *J. Biol. Chem.* **278,** 4536–4541
8. Tong, K. I., Katoh, Y., Kusunoki, H., Itoh, K., Tanaka, T., and Yamamoto, M. (2006) Keap1 recruits Neh2 through binding to ETGE and DLG motifs: characterization of the two-site molecular recognition model. *Mol. Cell. Biol.* **26,** 2887–2900
9. Ogura, T., Tong, K. I., Mio, K., Maruyama, Y., Kurokawa, H., Sato, C., and Yamamoto, M. (2010) Keap1 is a forked-stem dimer structure with two large spheres enclosing the intervening, double glycine repeat, and C-terminal domains. *Proc. Natl. Acad. Sci. U.S.A.* **107,** 2842–2847
10. McMahon, M., Itoh, K., Yamamoto, M., and Hayes, J. D. (2003) Keap1-dependent proteasomal degradation of transcription factor Nrf2 contributes to the negative regulation of antioxidant response element-driven gene expression. *J. Biol. Chem.* **278,** 21592–21600
11. Dinkova-Kostova, A. T., Holtzclaw, W. D., Cole, R. N., Itoh, K., Wakabayashi, N., Katoh, Y., Yamamoto, M., and Talalay, P. (2002) Direct evidence that sulfhydryl groups of Keap1 are the sensors regulating induction of phase 2 enzymes that protect against carcinogens and oxidants. *Proc. Natl. Acad. Sci. U.S.A.* **99,** 11908–11913
12. Yamamoto, T., Suzuki, T., Kobayashi, A., Wakabayashi, J., Maher, J., Motohashi, H., and Yamamoto, M. (2008) Physiological significance of reactive cysteine residues of Keap1 in determining Nrf2 activity. *Mol. Cell. Biol.* **28,** 2758–2770
13. Kensler, T. W., Wakabayashi, N., and Biswal, S. (2007) Cell survival responses to environmental stresses via the Keap1-Nrf2-ARE pathway. *Annu. Rev. Pharmacol. Toxicol.* **47,** 89–116
14. Wakabayashi, N., Dinkova-Kostova, A. T., Holtzclaw, W. D., Kang, M. I., Kobayashi, A., Yamamoto, M., Kensler, T. W., and Talalay, P. (2004) Protection against electrophile and oxidant stress by induction of the phase 2 response: fate of cysteines of the Keap1 sensor modified by inducers. *Proc. Natl. Acad. Sci. U.S.A.* **101,** 2040–2045
15. Itoh, K., Wakabayashi, N., Katoh, Y., Ishii, T., Igarashi, K., Engel, J. D., and Yamamoto, M. (1999) Keap1 represses nuclear activation of antioxidant responsive elements by Nrf2 through binding to the amino-terminal Neh2 domain. *Genes Dev.* **13,** 76–86
16. Nguyen, T., Nioi, P., and Pickett, C. B. (2009) The Nrf2-antioxidant response element signaling pathway and its activation by oxidative stress. *J. Biol. Chem.* **284,** 13291–13295
17. Nguyen, T., Yang, C. S., and Pickett, C. B. (2004) The pathways and molecular mechanisms regulating Nrf2 activation in response to chemical stress. *Free Radic. Biol. Med.* **37,** 433–441
18. Wang, X. J., Sun, Z., Villeneuve, N. F., Zhang, S., Zhao, F., Li, Y., Chen, W., Yi, X., Zheng, W., Wondrak, G. T., Wong, P. K., and Zhang, D. D. (2008) Nrf2 enhances resistance of cancer cells to chemotherapeutic drugs, the dark side of Nrf2. *Carcinogenesis* **29,** 1235–1243
19. Goldfarb, D., Hast, B. E., Wang, W., and Major, M. B. (2014) Spotlite: web application and augmented algorithms for predicting co-complexed proteins from affinity purification-mass spectrometry data. *J. Proteome Res.* **13,** 5944–5955
20. Hast, B. E., Cloer, E. W., Goldfarb, D., Li, H., Siesser, P. F., Yan, F., Walter, V., Zheng, N., Hayes, D. N., and Major, M. B. (2014) Cancer-derived mutations in KEAP1 impair NRF2 degradation but not ubiquitination. *Cancer Res.* **74,** 808–817
21. Lee, D. F., Kuo, H. P., Liu, M., Chou, C. K., Xia, W., Du, Y., Shen, J., Chen, C. T., Huo, L., Hsu, M. C., Li, C. W., Ding, Q., Liao, T. L., Lai, C. C., Lin, A. C., *et al.* (2009) KEAP1 E3 ligase-mediated downregulation of NF-κB signaling by targeting IKKβ. *Mol. Cell* **36,** 131–140
22. Lo, S. C., and Hannink, M. (2006) PGAM5, a Bcl-XL-interacting protein, is a novel substrate for the redox-regulated Keap1-dependent ubiquitin ligase complex. *J. Biol. Chem.* **281,** 37893–37903
23. Orthwein, A., Noordermeer, S. M., Wilson, M. D., Landry, S., Enchev, R. I., Sherker, A., Munro, M., Pinder, J., Salsman, J., Dellaire, G., Xia, B., Peter, M., and Durocher, D. (2015) A mechanism for the suppression of homologous recombination in G_1 cells. *Nature* **528,** 422–426
24. Kim, J. E., You, D. J., Lee, C., Ahn, C., Seong, J. Y., and Hwang, J. I. (2010) Suppression of NF-κB signaling by KEAP1 regulation of IKKβ activity through autophagic degradation and inhibition of phosphorylation. *Cell Signal.* **22,** 1645–1654
25. Barone, M. C., Sykiotis, G. P., and Bohmann, D. (2011) Genetic activation of Nrf2 signaling is sufficient to ameliorate neurodegenerative phenotypes in a *Drosophila* model of Parkinson's disease. *Dis. Model Mech.* **4,** 701–707
26. Kim, H. J., and Vaziri, N. D. (2010) Contribution of impaired Nrf2-Keap1 pathway to oxidative stress and inflammation in chronic renal failure. *Am. J. Physiol. Renal Physiol.* **298,** F662–671
27. Kim, J. H., Choi, Y. K., Lee, K. S., Cho, D. H., Baek, Y. Y., Lee, D. K., Ha, K. S., Choe, J., Won, M. H., Jeoung, D., Lee, H., Kwon, Y. G., and Kim, Y. M. (2012) Functional dissection of Nrf2-dependent phase II genes in vascular inflammation and endotoxic injury using Keap1 siRNA. *Free Radic. Biol. Med.* **53,** 629–640
28. Kim, M. S., Lee, W. S., and Jin, W. (2016) TrkB promotes breast cancer metastasis via suppression of Runx3 and Keap1 expression. *Mol. Cells* **39,** 258–265
29. Konstantinopoulos, P. A., Spentzos, D., Fountzilas, E., Francoeur, N., Sanisetty, S., Grammatikos, A. P., Hecht, J. L., and Cannistra, S. A. (2011) Keap1 mutations and Nrf2 pathway activation in epithelial ovarian cancer. *Cancer Res.* **71,** 5081–5089
30. Mann, G. E., Bonacasa, B., Ishii, T., and Siow, R. C. (2009) Targeting the redox sensitive Nrf2-Keap1 defense pathway in cardiovascular disease: protection afforded by dietary isoflavones. *Curr. Opin. Pharmacol.* **9,** 139–145
31. Ohta, T., Iijima, K., Miyamoto, M., Nakahara, I., Tanaka, H., Ohtsuji, M., Suzuki, T., Kobayashi, A., Yokota, J., Sakiyama, T., Shibata, T., Yamamoto, M., and Hirohashi, S. (2008) Loss of Keap1 function activates Nrf2 and provides advantages for lung cancer cell growth. *Cancer Res.* **68,** 1303–1309
32. Singh, S., Vrishni, S., Singh, B. K., Rahman, I., and Kakkar, P. (2010) Nrf2-ARE stress response mechanism: a control point in oxidative stress-mediated dysfunctions and chronic inflammatory diseases. *Free Radic. Res.* **44,** 1267–1288
33. Sykiotis, G. P., and Bohmann, D. (2008) Keap1/Nrf2 signaling regulates oxidative stress tolerance and lifespan in *Drosophila*. *Dev. Cell* **14,** 76–85
34. Sykiotis, G. P., and Bohmann, D. (2010) Stress-activated cap'n'collar transcription factors in aging and human disease. *Sci. Signal.* **3,** re3
35. Cancer Genome Atlas Research Network (2014) Comprehensive molecular profiling of lung adenocarcinoma. *Nature* **511,** 543–550
36. Cerami, E., Gao, J., Dogrusoz, U., Gross, B. E., Sumer, S. O., Aksoy, B. A., Jacobsen, A., Byrne, C. J., Heuer, M. L., Larsson, E., Antipin, Y., Reva, B., Goldberg, A. P., Sander, C., and Schultz, N. (2012) The cBio cancer genomics portal: an open platform for exploring multidimensional cancer genomics data. *Cancer Discov.* **2,** 401–404
37. Gao, J., Aksoy, B. A., Dogrusoz, U., Dresdner, G., Gross, B., Sumer, S. O., Sun, Y., Jacobsen, A., Sinha, R., Larsson, E., Cerami, E., Sander, C., and Schultz, N. (2013) Integrative analysis of complex cancer genomics and clinical profiles using the cBioPortal. *Sci. Signal.* **6,** pl1
38. Imielinski, M., Berger, A. H., Hammerman, P. S., Hernandez, B., Pugh, T. J., Hodis, E., Cho, J., Suh, J., Capelletti, M., Sivachenko, A., Sougnez, C., Auclair, D., Lawrence, M. S., Stojanov, P., Cibulskis, K., *et al.* (2012) Map-

ping the hallmarks of lung adenocarcinoma with massively parallel sequencing. *Cell* **150,** 1107–1120
39. Deegan, T. D., and Diffley, J. F. (2016) MCM: one ring to rule them all. *Curr. Opin. Struct. Biol.* **37,** 145–151
40. Remus, D., and Diffley, J. F. (2009) Eukaryotic DNA replication control: lock and load, then fire. *Curr. Opin. Cell Biol.* **21,** 771–777
41. Siddiqui, K., On, K. F., and Diffley, J. F. (2013) Regulating DNA replication in eukarya. *Cold Spring Harb. Perspect. Biol.* **5,** 9
42. Cortez, D., Glick, G., and Elledge, S. J. (2004) Minichromosome maintenance proteins are direct targets of the ATM and ATR checkpoint kinases. *Proc. Natl. Acad. Sci. U.S.A.* **101,** 10078–10083
43. Cheng, I. H., Roberts, L. A., and Tye, B. K. (2002) Mcm3 is polyubiquitinated during mitosis before establishment of the pre-replication complex. *J. Biol. Chem.* **277,** 41706–41714
44. Takei, Y., Assenberg, M., Tsujimoto, G., and Laskey, R. (2002) The MCM3 acetylase MCM3AP inhibits initiation, but not elongation, of DNA replication via interaction with MCM3. *J. Biol. Chem.* **277,** 43121–43125
45. Lecona, E., Rodriguez-Acebes, S., Specks, J., Lopez-Contreras, A. J., Ruppen, I., Murga, M., Munoz, J., Mendez, J., and Fernandez-Capetillo, O. (2016) USP7 is a SUMO deubiquitinase essential for DNA replication. *Nat. Struct. Mol. Biol.* **23,** 270–277
46. Wei, L., and Zhao, X. (2016) A new MCM modification cycle regulates DNA replication initiation. *Nat. Struct. Mol. Biol.* **23,** 209–216
47. Yeeles, J. T., Deegan, T. D., Janska, A., Early, A., and Diffley, J. F. (2015) Regulated eukaryotic DNA replication origin firing with purified proteins. *Nature* **519,** 431–435
48. Heller, R. C., Kang, S., Lam, W. M., Chen, S., Chan, C. S., and Bell, S. P. (2011) Eukaryotic origin-dependent DNA replication *in vitro* reveals sequential action of DDK and S-CDK kinases. *Cell* **146,** 80–91
49. Maculins, T., Nkosi, P. J., Nishikawa, H., and Labib, K. (2015) Tethering of SCF(Dia2) to the replisome promotes efficient ubiquitylation and disassembly of the CMG helicase. *Curr. Biol.* **25,** 2254–2259
50. Maric, M., Maculins, T., De Piccoli, G., and Labib, K. (2014) Cdc48 and a ubiquitin ligase drive disassembly of the CMG helicase at the end of DNA replication. *Science* **346,** 1253596
51. Dewar, J. M., Budzowska, M., and Walter, J. C. (2015) The mechanism of DNA replication termination in vertebrates. *Nature* **525,** 345–350
52. Moreno, S. P., Bailey, R., Campion, N., Herron, S., and Gambus, A. (2014) Polyubiquitylation drives replisome disassembly at the termination of DNA replication. *Science* **346,** 477–481
53. Tan, M. K., Lim, H. J., Bennett, E. J., Shi, Y., and Harper, J. W. (2013) Parallel SCF adaptor capture proteomics reveals a role for SCFFBXL17 in NRF2 activation via BACH1 repressor turnover. *Mol. Cell* **52,** 9–24
54. Wang, W., and Chan, J. Y. (2006) Nrf1 is targeted to the endoplasmic reticulum membrane by an N-terminal transmembrane domain. Inhibition of nuclear translocation and transacting function. *J. Biol. Chem.* **281,** 19676–19687
55. Zhang, Y., Crouch, D. H., Yamamoto, M., and Hayes, J. D. (2006) Negative regulation of the Nrf1 transcription factor by its N-terminal domain is independent of Keap1: Nrf1, but not Nrf2, is targeted to the endoplasmic reticulum. *Biochem. J.* **399,** 373–385
56. Watai, Y., Kobayashi, A., Nagase, H., Mizukami, M., McEvoy, J., Singer, J. D., Itoh, K., and Yamamoto, M. (2007) Subcellular localization and cytoplasmic complex status of endogenous Keap1. *Genes Cells* **12,** 1163–1178
57. Emanuele, M. J., Elia, A. E., Xu, Q., Thoma, C. R., Izhar, L., Leng, Y., Guo, A., Chen, Y. N., Rush, J., Hsu, P. W., Yen, H. C., and Elledge, S. J. (2011) Global identification of modular cullin-RING ligase substrates. *Cell* **147,** 459–474
58. Brewster, A. S., Wang, G., Yu, X., Greenleaf, W. B., Carazo, J. M., Tjajadi, M., Klein, M. G., and Chen, X. S. (2008) Crystal structure of a near-full-length archaeal MCM: functional insights for an AAA+ hexameric helicase. *Proc. Natl. Acad. Sci. U.S.A.* **105,** 20191–20196
59. Lam, S. K., Ma, X., Sing, T. L., Shilton, B. H., Brandl, C. J., and Davey, M. J. (2013) The PS1 hairpin of Mcm3 is essential for viability and for DNA unwinding *in vitro*. *PLoS ONE* **8,** e82177
60. Musahl, C., Holthoff, H. P., Lesch, R., and Knippers, R. (1998) Stability of the replicative Mcm3 protein in proliferating and differentiating human cells. *Exp. Cell Res.* **241,** 260–264
61. Drissi, R., Dubois, M. L., Douziech, M., and Boisvert, F. M. (2015) Quantitative proteomics reveals dynamic interactions of the minichromosome maintenance complex (MCM) in the cellular response to etoposide induced DNA damage. *Mol. Cell Proteomics* **14,** 2002–2013
62. Itoh, K., Tong, K. I., and Yamamoto, M. (2004) Molecular mechanism activating Nrf2-Keap1 pathway in regulation of adaptive response to electrophiles. *Free Radic. Biol. Med.* **36,** 1208–1213
63. Kobayashi, A., Kang, M. I., Watai, Y., Tong, K. I., Shibata, T., Uchida, K., and Yamamoto, M. (2006) Oxidative and electrophilic stresses activate Nrf2 through inhibition of ubiquitination activity of Keap1. *Mol. Cell. Biol.* **26,** 221–229
64. Takaya, K., Suzuki, T., Motohashi, H., Onodera, K., Satomi, S., Kensler, T. W., and Yamamoto, M. (2012) Validation of the multiple sensor mechanism of the Keap1-Nrf2 system. *Free Radic. Biol. Med.* **53,** 817–827
65. Mathew, R., Khor, S., Hackett, S. R., Rabinowitz, J. D., Perlman, D. H., and White, E. (2014) Functional role of autophagy-mediated proteome remodeling in cell survival signaling and innate immunity. *Mol. Cell* **55,** 916–930
66. Remus, D., Beuron, F., Tolun, G., Griffith, J. D., Morris, E. P., and Diffley, J. F. (2009) Concerted loading of Mcm2–7 double hexamers around DNA during DNA replication origin licensing. *Cell* **139,** 719–730
67. Snyder, M., He, W., and Zhang, J. J. (2005) The DNA replication factor MCM5 is essential for Stat1-mediated transcriptional activation. *Proc. Natl. Acad. Sci. U.S.A.* **102,** 14539–14544
68. Yankulov, K., Todorov, I., Romanowski, P., Licatalosi, D., Cilli, K., McCracken, S., Laskey, R., and Bentley, D. L. (1999) MCM proteins are associated with RNA polymerase II holoenzyme. *Mol. Cell. Biol.* **19,** 6154–6163
69. Chen, T., Zhou, T., He, B., Yu, H., Guo, X., Song, X., and Sha, J. (2014) mUbiSiDa: a comprehensive database for protein ubiquitination sites in mammals. *PLoS ONE* **9,** e85744
70. Sun, J., Evrin, C., Samel, S. A., Fernández-Cid, A., Riera, A., Kawakami, H., Stillman, B., Speck, C., and Li, H. (2013) Cryo-EM structure of a helicase loading intermediate containing ORC-Cdc6-Cdt1-MCM2–7 bound to DNA. *Nat. Struct. Mol. Biol.* **20,** 944–951
71. Costa, A., Ilves, I., Tamberg, N., Petojevic, T., Nogales, E., Botchan, M. R., and Berger, J. M. (2011) The structural basis for MCM2–7 helicase activation by GINS and Cdc45. *Nat. Struct. Mol. Biol.* **18,** 471–477
72. Bochman, M. L., Bell, S. P., and Schwacha, A. (2008) Subunit organization of Mcm2–7 and the unequal role of active sites in ATP hydrolysis and viability. *Mol. Cell. Biol.* **28,** 5865–5873
73. Samel, S. A., Fernández-Cid, A., Sun, J., Riera, A., Tognetti, S., Herrera, M. C., Li, H., and Speck, C. (2014) A unique DNA entry gate serves for regulated loading of the eukaryotic replicative helicase MCM2–7 onto DNA. *Genes Dev.* **28,** 1653–1666
74. Hast, B. E., Goldfarb, D., Mulvaney, K. M., Hast, M. A., Siesser, P. F., Yan, F., Hayes, D. N., and Major, M. B. (2013) Proteomic analysis of ubiquitin ligase KEAP1 reveals associated proteins that inhibit NRF2 ubiquitination. *Cancer Res.* **73,** 2199–2210
75. Camp, N. D., James, R. G., Dawson, D. W., Yan, F., Davison, J. M., Houck, S. A., Tang, X., Zheng, N., Major, M. B., and Moon, R. T. (2012) Wilms tumor gene on X chromosome (WTX) inhibits degradation of NRF2 protein through competitive binding to KEAP1 protein. *J. Biol. Chem.* **287,** 6539–6550
76. Kim, T. Y., Siesser, P. F., Rossman, K. L., Goldfarb, D., Mackinnon, K., Yan, F., Yi, X., MacCoss, M. J., Moon, R. T., Der, C. J., and Major, M. B. (2015) Substrate trapping proteomics reveals targets of the βTrCP2/FBXW11 ubiquitin ligase. *Mol. Cell. Biol.* **35,** 167–181
77. Vizcaíno, J. A., Deutsch, E. W., Wang, R., Csordas, A., Reisinger, F., Ríos, D., Dianes, J. A., Sun, Z., Farrah, T., Bandeira, N., Binz, P. A., Xenarios, I., Eisenacher, M., Mayer, G., Gatto, L., *et al.* (2014) ProteomeXchange provides globally coordinated proteomics data submission and dissemination. *Nat. Biotechnol.* **32,** 223–226